ARCHIVES OF MECHANICS
Arch. Mech. **75** (1-2), 169–211, 2023, DOI: 10.24423/aom.4139

Analysis of time-averaged secondary flow cells in wide and narrow straight open channels with lateral bed deformation

T. CHATTOPADHYAY, S. KUNDU

Department of Mathematics, NIT Jamshedpur, Jharkhand-831014, India,
e-mails: chatterjeetitas1610@gmail.com, snehasis.math@nitjsr.ac.in

The usual cellular pattern of the time averaged secondary flow circulation in the central section of wide open channels shows a distorted (laterally or vertically) structure due to the changes in bed configurations along lateral direction. The structures of these secondary circulations (under different bed configurations) are crucial for different types of hydraulic modeling. This study presents mathematical models of the time averaged secondary velocities (lateral and vertical components) for a turbulence-induced secondary current at the central section of a wide open-channel flow under different types of elevated and non-elevated bed conditions. Starting with the Reynolds Averaged Navier-Stokes equation and using the continuity equation, at first the governing equation of secondary flow velocity is obtained including the effects of the eddy viscosity and viscosity of the fluid. The model equations is solved using a separation of the variable technique imposing the bed perturbation condition. Full analytical solutions are achieved through mathematical analysis using suitable boundary conditions consistent with experimental observations. Initially the models are derived for a non-elevated bedforms comprised of alternating equal widths of smooth and rough bed strips. These models are modified further for bedforms with unequal widths of rough and smooth bed strips and elevated periodic bed structures. Four different types of elevated bed configurations are investigated and a general approach is suggested for other types of bed forms. All the proposed models are validated with existing experimental results to ensure the applicability and in each cases, improved results are observed. Obtained results show that the centre of circulation of the cellular structure occurs above the junction of the rough and smooth bed strips (consistent with experimental observations) and it gradually shifts towards the smooth strip, when the length of the rough bed strip is increased. The shifting as a function shows a non-linear pattern with the length of the rough bed strip. A least-square model is proposed to identify the circulation center as a function of the ratio of rough to smooth bed strips. It is also found that the vertically distorted secondary cells are generated when the bed slope strictly increase/decrease throughout the length of the one whole circulation. Finally, all the proposed models are compared with an existing model and an error analysis is done. Results of error analysis show that the present study can be more suitable as it yields improved results.

Key words: turbulent flow, secondary currents, method of separation of variable, Reynolds shear stress.

Notation

A	empirical constant,
B	width of the channel,
b	bed function,
C_1, C_* and C_{**}	constants,
g	gravitational acceleration ($\approx 9.81\,\mathrm{m/s}$),
h	flow height,
J_l	longitudinal channel slope,
N	number od data points,
p, q, r	main, transverse and vertical velocity profiles,
p', q', r'	fluctuating main, transverse and vertical velocity profiles,
F	amplitude of perturbation function,
G	a periodic function,
L	constant,
l	$\overline{u_*}/R_{\max}$,
P	pressure,
PS, PC	modified periodic functions,
R_0	designated to secondary current component without bed elevation,
R_1	designated to perturbed flow,
$R_{\max}$	maximum up-welling velocity,
t	time,
u_*	shear velocity,
U_m	mean primary flow velocity,
v_{cp}	computed velocity,
v_{ob}	observed velocity,
x, y, z	main, transverse and vertical Coordinate axis,
z_0	zero primary flow velocity level,
α	dip correction parameter,
ν	kinematic viscosity,
ν_t	Eddy viscosity,
κ	von Karman coefficient,
Π	Coles wake parameter,
∇	Laplacian operator,
ρ	fluid density,
λ	mean width of the bed strip $= \frac{\lambda_{up}+\lambda_{dn}}{2}$,
λ_{up}	width of the up-flow zone,
λ_{dn}	width of the down-flow zone,
λ_r	width of the rough bed strip,
λ_s	width of the smooth bed strip,
λ_*	parameter for bed perturbation of bed elevation,
λ_1	$\pi\sqrt{\lvert\Xi\rvert/2\Sigma}$,
Ξ	$\tilde{\nu} + \overline{\tilde{\nu}_t}$,
Σ	$2(\tilde{\nu} - \overline{\tilde{\nu}_t})$,
Φ	function of $\tilde{y}$ and $\tilde{z}$,
ψ	stream function,
$\overline{(.)}$	the mean of the components,
$\tilde{(.)}$	dimensionless components.

1. Introduction

Secondary flows are omnipresent in natural and artificial open channel turbulent flows. The classification of secondary flows was first proposed by Prandtl [1]. Due to the curvilinearity of the streamlines, the consequences of the mean flow skewness can be seen in secondary currents which are called Prandtl's first kind, and the non-uniformities in the flow near to wall boundary regions induced by anisotropy of turbulence are called Prandtl's second kind. Prandtl [1] also reported that the first kind is induced by the asymmetrical mean flow in curved channels as well as the drifting rivers and this type of secondary flow can be seen in both the laminar and the turbulent flows. The second kind is caused by the non-homogeneity of the turbulence and it is also known as shear or turbulence-driven secondary flow. Modeling and understanding the flow structure and determination of secondary velocities along the vertical and transverse directions in a wide-open channel helps to understand the transportation of sediments, variation of the shear stress on the bed surface, distribution of the turbulent shear stress, and settling velocity distribution of sediment particles in flow along the lateral direction. Several experimental studies exist on the structure of secondary flow cells under various types of bed conditions, though proper mathematical formulations and models are limited [2–5]. Therefore more generalized mathematical approach and a model under the different elevated and non-elevated beds in wide open channels are needed.

Open channels are classified as narrow and wide according to the value of the aspect ratio defined as $Ar = b/h$ (b = channel width, h = channel depth). When the aspect ratio $Ar < 5$, the channel is described as a narrow open channel. Otherwise, it is called a wide open channel [6]. The existence of the secondary flow in the open channel had been investigated by various researchers such as Stearns [7], Francis [8], Gibson [9], Thomson [10]. Though secondary currents are seen in both these types of open channels, their mechanism of generation is different. The characteristics of secondary currents in narrow open channels were envisaged and investigated by Naot and Rodi [11] and Gibson [9]. The secondary flow observed in the narrow open channel is composed of a free surface vortex and bottom vortex which causes the 'corner flows' [12]. Several researchers in the 1980s discovered that the secondary currents can be generated without the 'corner flows', with slightly perturbed channel beds. The experimental results by Nezu and Rodi [2] and Wang and Cheng [13] showed that the lateral variation in the bed topography and bed surface roughness can lead to the generation of the secondary flow cell. These types of secondary currents are free from the sidewall effects of the channels [4, 14]. In wide open channels sidewall effects are diminished gradually from the sidewall to the central section and secondary

currents can be generated with changes in the bed configuration and roughness along the lateral direction. The lateral variation of the bed configuration develops periodic streamwise vortices which have a dimension equal to the flow depth of the channel [4]. These streamwise vortices appear as a pair of counter-rotating cells of a total span of twice the flow depth [5, 15]. In straight wide open channels this type of secondary flow can be seen throughout the whole cross-section. The existence of spanwise secondary current in a wide-open channel was discovered by Vanoni [16]. Coleman [17] observed the high sediment flow zone along the streamwise direction, known as the "line of boil", in natural resources. He further observed that the lines of boil occur periodically and between two lines of boils a low suspension zone exists. This observation also concludes the existence of periodic secondary currents in wide rivers. Further, Kinoshita [18] found that the secondary currents in the streamwise direction consist of two counter-rotating vortices with a diameter equal to the flow depth and having a spanwise spacing of twice the flow depth.

In all types of open channel flows under different channel geometry, velocity always has three components. These velocity components are functions of lateral and vertical coordinates in a uniform flow along the main streamwise flow direction. In natural rivers and canals, the bed consists of sediments that continuously move with flow under the bedload. As a result, bedforms occur (bed troughs and bed ridges). These bed troughs and ridges generate cellular secondary current cells. Experimental results of Wang and Cheng [5] further suggest that alternately arranged equal and unequal length of non-elevated smooth and rough bed surfaces also generates similar secondary flow cells. These cellular circulations consist of up-flow and down-flow regions. These secondary currents change the distributions of turbulent shear stress and the primary flow velocity in up-flow and down-flow regions. The extensive studies of Yang *et al.* [19], Yang [20] and Kundu and Ghoshal [21] showed that the vertical component of the secondary current changes the distribution of the turbulent shear stress form the traditionally accepted linear type profile. As a result, the zero Reynolds shear stress occurs below the free surface. The existence of the vertically downward secondary flow velocity results in the zero shear stress point shifting downward from the free surface [21]. The changes in the position of zero shear stress point from the free surface cause the velocity dip-phenomenon [19]. Apart from this, the deviation of the turbulent shear stress distribution from the linear profile in a wide open channel with alternate rough and smooth bed forms was proposed by [14]. Results of Wang and Cheng [14] show that a convex type profile in the up-flow zone and a concave type profile in the down-flow zone may occur which suggests the existence of a non-linear pattern of the shear stress distribution. Apart from the results of the Reynolds shear stress distribution, a recent study of Mohan *et al.* [22] has shown that the transverse velocity distribution depends

on the formation of circular vortex in the cross-sectional plane and becomes periodic as the number of the circular vortex increases for an increasing aspect ratio.

Due to the existence of erodible sediment beds in natural alluvial rivers, elevated bed forms occur. Therefore, careful consideration of different types of elevated bedforms and analysis of the structure of secondary circulations are essential elements of open-channel hydraulics. The knowledge and prediction of such secondary cells help to give an idea about their effect on other hydraulic components. Experimental observations on vertical secondary velocity data from Ohmoto *et al.* [23], Soualmia *et al.* [24] and Ghoshal *et al.* [25] reveal that the maximum value of vertical secondary velocity may not always occur at the middle of the flow depth. Thus existing empirical models need careful improvements. Most of the previously proposed models of the secondary current are developed using experimental data as well as theoretical with some semi-empirical or empirical results. The models of secondary velocities that were proposed before the year 2006, can only be applied to predict secondary velocities in non-elevated bedforms. The experiments of Nezu and Nakagawa [15] and Wang and Cheng [5] suggest the structures of secondary cells change when non-elevated bed strips (rough and smooth) of unequal lengths or elevated bed forms are used. Further Wang and Cheng [5] showed that the structures of cellular cells change under different bedforms. Wang and Cheng [5] proposed models for secondary current using an empirical stream function that applies only to wavy ridges and always predicts maximum vertical velocity at the middle of flow depth for non-elevated bed conditions. Recently Kundu *et al.* [26] and Kundu and Chattopadhyay [27] have investigated the secondary velocity only for equal and unequal non-elevated bed conditions. Till now, the models of secondary current for different types of elevated bed forms/ridges are missing in the literature, which gives the major motivation for the present investigation. In Table 1 the applicability and limitation of existing models in literature along with proposed models are given to give a more clear idea. Further, since the numerical computations are computationally expensive and complex from an applications perspective, efforts need to be given for an analytical approach.

The leading objectives of this study are (a) to find the analytical models for profiles of the secondary flow velocities in turbulent flow through wide open channels under elevated as well as non-elevated bed conditions; (b) to study the effects of bed elevation on the contours of secondary cells; (c) to validate all the proposed models with the experimental data and compare with previous models; (d) to investigate the structures of cellular secondary cells under some different bed structures; (e) to study the effects of bed structure on the location of the center of circulation.

Table 1. Details and limitations of empirical/semi-empirical models of stream in literature along with proposed model

Authors	Applicable bed forms	Mathematical model	Limitations
Ikeda [3]	Non-elevated equal length bed-strips	$\tilde{\psi} = -\frac{6A_b}{\kappa\pi^3}[(2\tilde{z}-1)\cos(\pi\tilde{z})+1]\sin(\pi\tilde{y})$	This model does not contain effect of viscosity.
Kotsovinos [35]	Non-elevated equal length bed-strips	$\tilde{\psi} = -A\sin(\pi\tilde{z})\sin(\pi\tilde{y})$	Effects of bed roughness and viscosity effects are not included.
Wang and Cheng [5]	Non-elevated equal length bed-strips (cellular secondary cells)	$\tilde{\psi} = -\frac{1}{\pi}\sin(\pi\tilde{z})\sin(\pi\tilde{y})$	Semi-empirical model proposed based on the empirical form of the stream function.
Wang and Cheng [5]	Non-elevated unequal bed-strips (laterally skewed flow cells)	$\tilde{\psi} = -\frac{1}{\pi}\sin(\pi\tilde{z})PS(\tilde{y})$	Semi-empirical model proposed based on the empirical form of the stream function. These models gave the experimental results which are only validated for the non-elevated bed forms of unequal lengths.
Wang and Cheng [5]	Elevated wavy ridges	$\tilde{\psi} = -\frac{1}{\pi}\sin\left(\pi\frac{\tilde{z}-b}{h}\right)PS(\tilde{y})$	Semi-empirical model proposed based on the empirical form of the stream function. Model gives secondary velocity to only wavy ridges type of elevated bed forms.
Kundu *et. al.* [26]	Non-elevated equal smooth and rough bed-strip configuration	$\tilde{\psi}(\tilde{y},\tilde{z}) = \frac{1}{\pi}\left\{\frac{-K_b(1+\alpha)}{2\Lambda}[\tilde{z}-\tilde{z}^2]+C_1\sin(\pi\tilde{z})\right\}\sin(\pi\tilde{y}),$ $C_1 = \left[-\widetilde{W}_{\max}+\frac{K_b(1+\alpha)}{8\Lambda}\right]$	Includes effects of fluid viscosity and eddy diffusivity. Applicable only in wide open-channel with symmetric smooth and rough non-elevated bed forms.

Table 1. [cont.]

Authors	Applicable bed forms	Mathematical model	Limitations
Kundu *et. al* [26]	Non-elevated unequal smooth and rough bed-strip configuration	$\tilde{\psi}(\tilde{y},\tilde{z}) = \frac{1}{\pi}\left\{\frac{-K_b(1+\alpha)}{2\Lambda}[\tilde{z}-\tilde{z}^2]+C_1\sin(\pi\tilde{z})\right\}PS(\pi\tilde{y}),$ $C_1 = \left[-\widetilde{W}_{max}+\frac{K_b(1+\alpha)}{8\Lambda}\right]$	Includes effects of fluid viscosity and eddy diffusivity. Applicable in wide open-channel with unequal smooth and rough non-elevated bed forms.
Proposed model	Equal and non-elevated rough and smooth bed-strips	$\tilde{\psi} = \frac{\ell}{\pi}C_1\sin(\pi\tilde{z})\sin(\pi\tilde{y})+\frac{\ell L\lambda_*}{\pi^5}\sin(\pi\tilde{y})\Big[\cos(\lambda_1\tilde{z})$ $-C_{**}\frac{\sin(\lambda_1\tilde{z})}{\sin\lambda_1}+\tilde{z}\Big[C_*\cos(\lambda_1\tilde{z})$ $+\frac{\lambda_1}{2}\sin(\lambda_1\tilde{z})\Big]+(2\tilde{z}-1)\Big]$	Derived from RANS equation applicable for different type of natural bed forms by including fluid viscosity and bed perturbation effects.
Proposed model	Unequal and non-elevated rough and smooth bed-strips	$\tilde{\psi}(\tilde{y},\tilde{z}') = \Big[\frac{\ell}{\pi}C_1\sin(\pi\tilde{z}')+\frac{\ell L\lambda_*}{\pi^5}\Big[\cos(\lambda_1\tilde{z}')$ $-C_{**}\frac{\sin(\lambda_1\tilde{z}')}{\sin\lambda_1}+\tilde{z}'\Big[C_*\cos(\lambda_1\tilde{z}')$ $+\frac{\lambda_1}{2}\sin(\lambda_1\tilde{z}')\Big]+(2\tilde{z}'-1)\Big]\Big]PS(\tilde{y})$	Derived from RANS equation applicable for different type of natural bed forms by including fluid viscosity and bed perturbation effects.
Proposed model	Unequal and elevated bed forms of different types	$\tilde{\psi}(\tilde{y},\tilde{z}') = \Big[\frac{\ell}{\pi}C_1\sin(\pi\tilde{z}')+\frac{\ell L\lambda_*}{\pi^5}\Big[\cos(\lambda_1\tilde{z}')$ $-C_{**}\frac{\sin(\lambda_1\tilde{z}')}{\sin\lambda_1}+\tilde{z}'\Big[C_*\cos(\lambda_1\tilde{z}')+\frac{\lambda_1}{2}\sin(\lambda_1\tilde{z}')\Big]$ $+(2\tilde{z}'-1)\Big]\Big]PS(\tilde{y})$	Analytically derived from RANS equation applicable for different type of natural bed forms by including fluid viscosity and bed perturbation effects.

2. Main governing equation

In the late 1980s, researchers found if the channel bed is slightly perturbed the secondary currents can also be generated without "corners" in wide open channels. Nezu and Rodi [2] had given an experimental explanation of the lateral dissimilarities in bed topography and also pointed out the significant differences of secondary flows in both types of channels. It is necessary to clarify further these differences in characteristics of turbulence between these two types of flows because the anisotropic behavior of turbulence generates secondary currents and these are independent of the sidewall effect [4, 14].

Considering Prandtl's secondary currents of the second kind, the governing equation for steady and consistent turbulent flow in a straight and wide open rectangular-shaped channel is contemplated. Figure 1 shows the illustrative diagram of the assumptions for the case of an elevated longitudinal bed condition. Since secondary flow cells appear as counter-rotating circular type vortices with a span of twice the flow depth apart in a periodic manner (due to the presence of alternative 'sand ridges' and 'sand troughs') [4], therefore, in our present study, it is assumed that the formation of bed is periodical and it is comprised of fine and rough sands. Since in a wide open channel secondary cells can be generated either by variation of bed roughness or bed elevation [5], we consider both the cases of non-elevated and elevated beds. In the first case, the sand bed is not erodible (which can be made by fixing smooth and rough surfaces over the channel bottom as presented in Wang and Cheng [5]. In the next case, sand particles are considered erodible which during the flow, forms sand troughs (composed of fine sand particles) and sand ridges (composed of rough sand particles).

Figure 1 shows the up flow and down flow zones over the sand ridges and sand troughs, respectively as observed in several experiments. Here λ_{up} and λ_{dn} denote the half lengths of the up flow and down flow zones respectively and λ is the mean width of the bed strip. It is to be noted that this configuration of the bed is to initiate the problem formulation. Other different scenerios can be generated upon this configuration. For example, by varying the lengths of λ_{up} and λ_{dn} different bed structures can be obtained for the first case and by changing the bed function, different bed forms that appear in real flows can be obtained which is discussed towards the end of the manuscript. The main flow is considered along the x direction and y and z denote the lateral and vertical directions where the origin is considered at the central part of the channel. The continuity equation and the Reynolds averaged Navier–Stokes momentum equations along y and z directions are expressed as:

$$q_y + r_z = 0 \tag{2.1}$$

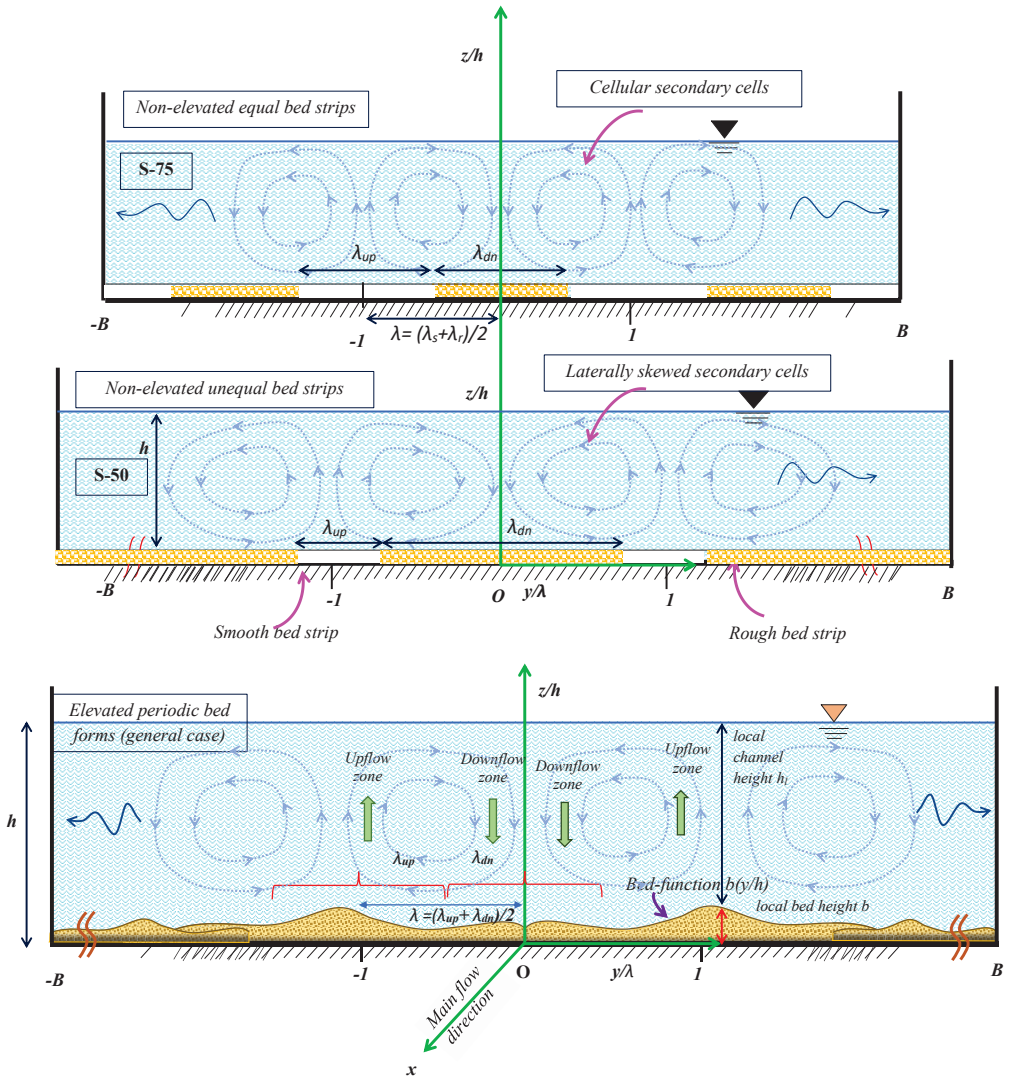

FIG. 1. Schematic diagram of cellular secondary cells wide-open channel with equal and unequal with non-elevated (equal and unequal length of bed strops) and elevated bed configurations.

and

$$q_t + qq_y + rq_z = -\frac{1}{\rho}P_y + \nu\nabla^2 q + \left[\frac{\partial}{\partial y}(-\overline{q'^2}) + \frac{\partial}{\partial z}(-\overline{q'r'})\right], \tag{2.2}$$

$$r_t + qr_y + rr_z = -gJ_l - \frac{1}{\rho}P_z + \nu\nabla^2 r + \left[\frac{\partial}{\partial y}(-\overline{q'r'}) + \frac{\partial}{\partial z}(-\overline{r'^2})\right], \tag{2.3}$$

where g as gravitational acceleration, ν is the kinematic viscosity, t indicates time, J_l is considered as longitudinal channel slope, P is the pressure, ρ is the fluid density. Fluctuating velocity components are denoted by the primes and the suffix denotes the partial derivatives. Since the flow through open channels is mainly governed by gravity, therefore by eliminating the pressure gradient term and differentiating the obtained equation concerning y the above equations we get the governing equation after simplification as

$$D_*\nabla^2 r = \frac{\partial^3}{\partial y^2 \partial z}(\overline{q'^2} - \overline{r'^2}) + \left(\frac{\partial^2}{\partial z^2} - \frac{\partial^2}{\partial y^2}\right)\frac{\partial}{\partial y}\overline{q'r'}, \tag{2.4}$$

where D_* is an operator defined as $\left(\frac{\partial}{\partial t} - \nu\nabla^2\right)$ in which ∇^2 indicates the Laplacian operator in two variables. To find the analytical solution of Eq. (2.4) for the vertical velocity component r, closures for the turbulent shear stress $\overline{q'r'}$ and the normal stresses $\overline{q'^2}$ and $\overline{r'^2}$ are required. WANG and CHENG [14] performed experiments with alternative smooth and rough bedforms in wide open channel flows. Their observation correlates the secondary circulation with smooth and rough bed strips. They also observed that the distribution of the dimensionless turbulent shear stress $-\frac{\overline{p'r'}}{u_*^2}$ changes with bed roughness. They reported a transition of turbulent shear stress forms an upward convex profile to an upward concave profile which transforms gradually along a transverse direction with increasing roughness. The theoretical configuration assumed in this study matches with the experiments of [14], the turbulent shear stress is modeled in this study after including the effects of bed roughness and following [27] as

$$\frac{\overline{q'^2} - \overline{r'^2}}{u_*^2} = \frac{-\overline{p'r'}}{u_*^2} = \left(1 - \frac{z}{h}\right)\left[1 - \alpha\pi\left\{\frac{z}{h}\right\}\cos\left(\frac{\pi y}{\lambda}\right)\right], \tag{2.5}$$

where α indicates the dip correction parameter and it signifies the magnitude of secondary current that can be determined from the experimental data. KUNDU and CHATTOPADHYAY [27] validated Eq. (2.5) with observations of [14] and find a good agreement with experimental data for the values of $\alpha = 0.2$. It is needful to mention here that for other types of bed configurations, its value can be obtained from the observational data. In the present study, $\alpha = 0.2$ is taken as the fixed parameter. Further, the Reynolds shear stress $-\overline{q'r'}$ can be expressed by the eddy viscosity models as [28]

$$-\overline{q'r'} = \nu_t\left(\frac{\partial q}{\partial z} + \frac{\partial r}{\partial y}\right), \tag{2.6}$$

where ν_t denotes the eddy viscosity which IKEDA [3] considered as $\nu_t = (k\overline{u}_* h)/6$, a constant after considering the logarithmic law of primary velocity as in which

$\overline{u}_*$ is the averaged shear velocity along the transverse direction. Existing reports in literature state that in such complex flows where secondary circulations occur, cannot be described by the logarithmic law [29–31]. Recently, PATEL *et al.* [31] have proposed the second log-wake law for open channel flows which can describe data well. Following IKEDA [3] and [31], the depth-averaged eddy viscosity model is expressed as:

$$\overline{\nu_t} = \kappa \overline{u}_* h \int_0^1 \left(\frac{2}{1-\tilde{z}^2} + \pi \Pi \frac{\sin(\pi \tilde{z})}{\tilde{z}} \right)^{-1} d\tilde{z}, \tag{2.7}$$

where Π is the Cole's wake parameter whose value is taken as 0.2 in this study [28].

Using Eqs. (2.6) and (2.5), the simplified governing equation is expressed form Eq. (2.4) as [26, 27]

$$D_* \nabla^2 r = \left[\frac{u_*^2}{\lambda^2 h} \alpha \pi^3 \cos\left(\pi \frac{y}{\lambda}\right) \left(1 - 2\frac{z}{h}\right) \right] + \overline{\nu_t} \left(\frac{\partial^4 r}{\partial z^4} - 2\frac{\partial^4 r}{\partial y^2 \partial z^2} + \frac{\partial^4 r}{\partial y^4} \right). \tag{2.8}$$

To make dimensionless Eq. (2.8), we introduce the following variables. In such studies, the velocity component is usually made dimensionless by the shear or friction velocity u_* which depends on the bed shear stress. Since, due to the variation of the bed roughness along the lateral direction, the shear velocity also changes along the lateral direction [14]. IKEDA [3] considers the average shear velocity to make dimensionless the secondary components of the velocity. So in the present study velocity components r and q are made dimensionless at the initial stage. The vertical coordinate is made dimensionless with the flow depth h for the case of non-elevated bedforms and the case of elevated bedforms, the maximum value of the flow depth has been used. Along the lateral direction, secondary currents are comprised of up-flow and down-flow zones which have lengths λ_{up} and λ_{dn}, respectively. These lengths can vary depending on the bed configuration. Therefore, the mean of these two lengths is used to make dimensionless the lateral coordinate. For other variables, the dimensionless quantities are defined as follows as:

$$\tilde{r} = \frac{r}{\overline{u}_*}, \quad \tilde{q} = \frac{q}{\overline{u}_*}, \quad \tilde{y} = \frac{y}{\lambda}, \quad \tilde{z} = \frac{z}{h}, \quad \tilde{t} = \frac{t\overline{u}_*}{h}, \quad \tilde{\overline{\nu_t}} = \frac{\tilde{\nu_t}}{\overline{u}_* h}, \quad \tilde{\nu} = \frac{\tilde{\nu}}{\overline{u}_* h}, \tag{2.9}$$

where h is the flow height, Here in this study λ is the same as the average width of the strip [5] which is defined as $\frac{\lambda_{up}+\lambda_{dn}}{2}$. Substituting the above non-dimensional quantities in Eq. (2.5) we get the dimensionless governing equation in the following form such as:

$$\tilde{D}_* \nabla^2 \tilde{r} = \alpha \pi^3 \cos(\pi \tilde{y})(1 - 2\tilde{z}) + \tilde{\overline{\nu_t}} \left(\frac{\partial^4 \tilde{r}}{\partial \tilde{z}^4} - 2\frac{\partial^4 \tilde{r}}{\partial \tilde{y}^2 \partial \tilde{z}^2} + \frac{\partial^4 \tilde{r}}{\partial \tilde{y}^4} \right). \tag{2.10}$$

Under the steady flow condition, Eq. (2.10) can be modified as:

$$(\tilde{\nu}+\overline{\tilde{\nu}_t})\frac{\partial^4\tilde{r}}{\partial\tilde{z}^4}+2(\tilde{\nu}-\overline{\tilde{\nu}_t})\frac{\partial^4\tilde{r}}{\partial\tilde{y}^2\partial\tilde{z}^2}+(\tilde{\nu}+\overline{\tilde{\nu}_t})\frac{\partial^4\tilde{r}}{\partial\tilde{y}^4}=-\alpha\pi^3\cos(\pi\tilde{y})(1-2\tilde{z}). \tag{2.11}$$

Equation (2.11) denotes the main governing equation for vertical velocity component $\tilde{r}$ of the secondary current. Due to the presence of the fluid viscosity terms, this model can also be extended for sediment-laden flow replacing the fluid viscosity with the viscosity of the mixing fluid. To get an analytical solution, suitable boundary conditions are employed from the experimental observations.

The cellular structure of secondary currents appears as counter-rotating vortices which have the size of the full flow depth [4]. But at the channel bottom as well as the free surface, the vertical velocity component vanishes. This conclusion is also drawn by YANG *et al.* [32] and by WANG and CHENG [5] in their experiments. Also, it has been observed that the vertical velocity becomes maximum almost at the middle of the flow depth at different sections along lateral direction [5]. Starting with the zero velocity the vertical velocity gradually increases till the middle of the flow depth and then decreases towards the free surface level (where the maximum velocity appears at some certain heights, the modified condition can be considered. This is further discussed in Section 6). The maximum value of vertical velocity always occurs where there is only up flow or down flow velocity occurs which generally occurs at the middle length of λ_{up} or λ_{dn}. Further, the experimental observations of NEZU and NAKAGAWA [15], NEZU and RODI [2] and WANG and CHENG [5] suggest that near the bed and free surface, the vertical velocity changes as a linear function of the vertical coordinate. Considering all these, the physical boundary conditions are taken as follows:

$$\begin{gathered}\tilde{r}\big|_{\tilde{z}=0}=0,\quad \tilde{r}\big|_{\tilde{z}=1}=0,\\ \tilde{r}\big|_{|\tilde{y}|=1,\tilde{z}=1/2}=\widetilde{R}_{\max},\quad \text{or}\quad \left.\frac{\partial\tilde{r}}{\partial\tilde{z}}\right|_{\tilde{z}=1/2}=0,\\ \left.\frac{\partial^2\tilde{r}}{\partial\tilde{z}^2}\right|_{\tilde{z}=0}=0,\quad \left.\frac{\partial^2\tilde{r}}{\partial\tilde{z}^2}\right|_{\tilde{z}=1}=0,\end{gathered} \tag{2.12}$$

where $\widetilde{R}_{\max}=R_{\max}/\overline{u}_*$ is the non-dimensional maximum vertical velocity.

3. Complete analytical solution

WANG and CHENG [14] showed that the flow that includes secondary currents is comprised of a 'base flow' and a 'perturbation part' which is caused by different reasons such as a change in bed roughness, change in bed elevation, and

others. This further implies that the ideal flow velocity part is disturbed by the bed perturbation. Therefore, introducing the bed perturbation parameter, the solution of Eq. (2.11) can be written as a linear superposition of two unknown functions $\tilde{R}_0(\tilde{y},\tilde{z})$ and $\tilde{R}_1(\tilde{y},\tilde{z})$ as [26]

$$\tilde{r} = \tilde{R}_0 + \lambda_* \tilde{R}_1, \tag{3.1}$$

where $\tilde{R}_0$ is idealized for the secondary flow and $\tilde{R}_1$ for the perturbed flow, λ_* is a parameter that signifies the bed perturbation of bed elevation. In our study, the bed perturbation is periodic in a manner (due to alternate variations of bed configuration). In such case, Eq. 3.1 can be rewritten in the following way:

$$\tilde{r} = \tilde{R}_0 + \lambda_* F(\tilde{z}) G(\tilde{y}). \tag{3.2}$$

Here $F(\tilde{z})$ represented the amplitude of perturbation and $G(\tilde{y}) = \cos(\pi\tilde{y})$ a periodic cosine function to characterize the lateral distributions of the stream-wise velocity and the Reynolds shear stress. The choice of $G\,(\tilde{y})$ as a cosine function was obtained from the experimental data of [14]. Since in the present study, a similar bed configuration is assumed, we have chosen $G(\tilde{y})$ as the same cosine function. To find the analytical solution to the definite problem we decomposed it into two sub-problems with suitable boundary conditions

$$\text{(I)} \quad \Sigma\frac{\partial^4\tilde{R}_1}{\partial\tilde{z}^4} + \Xi\frac{\partial^4\tilde{R}_1}{\partial\tilde{y}^2\partial\tilde{z}^2} + \Sigma\frac{\partial^4\tilde{R}_1}{\partial\tilde{y}^4} = -\tilde{\Phi}(\tilde{y},\tilde{z}), \tag{3.3}$$

where $\Sigma = (\tilde{\nu} + \overline{\tilde{\nu}_t})$ and $\Xi = 2(\tilde{\nu} - \overline{\tilde{\nu}_t})$. The suitable boundary conditions for sub-problem I are in the form of $\tilde{R}_1|_{\tilde{z}=0} = 0$, $\tilde{R}_1|_{\tilde{z}=1} = 0$, $\frac{\partial^2\tilde{R}_1}{\partial\tilde{z}^2}|_{\tilde{z}=0} = 0$, $\frac{\partial^2\tilde{R}_1}{\partial\tilde{z}^2}|_{\tilde{z}=1} = 0$, and $\frac{\partial\tilde{R}}{\partial\tilde{z}}|_{\tilde{z}=1/2} = 0$ and

$$\text{(II)} \quad \Sigma\frac{\partial^4\tilde{R}_0}{\partial\tilde{z}^4} + \Xi\frac{\partial^4\tilde{R}_0}{\partial\tilde{y}^2\partial\tilde{z}^2} + \Sigma\frac{\partial^4\tilde{R}_0}{\partial\tilde{y}^4} = 0. \tag{3.4}$$

The suitable boundary conditions for the sub-problem (II) are $\tilde{R}_0|_{\tilde{z}=0} = 0$, $\tilde{R}_0|_{\tilde{z}=1} = 0$ and $\frac{\partial\tilde{R}_0}{\partial\tilde{z}}|_{\tilde{z}=1/2} = 0$.

Solving the subproblem I analytically with suitable boundary conditions, finally we get the solution as (see Appendix for the detailed solution),

$$\tilde{R}_1 = \frac{L}{\pi^4}\cos(\pi\tilde{y})\left[\cos(\lambda_1\tilde{z}) - C_{**}\frac{\sin(\lambda_1\tilde{z})}{\sin\lambda_1} + \tilde{z}\left[C_*\cos(\lambda_1\tilde{z}) + \frac{\lambda_1}{2}\sin(\lambda_1\tilde{z})\right]\right], \tag{3.5}$$

where $L = \frac{\alpha_0\alpha\pi^3}{\Sigma}$ and $\lambda_1 = \pi\sqrt{\frac{|\Xi|}{2\Sigma}}$ (see Appendix for the detailed solution). C_{**} and C_* denoted as:

$$C_* = \left(\frac{2\lambda_1 - \lambda_1\sin^2(\lambda_1/2) + \frac{\lambda_1^2}{4}\sin\lambda_1 - 4\sin(\lambda_1/2)}{\lambda_1\cos\lambda_1 - \sin\lambda_1 - \lambda_1\sin^2(\lambda_1/2)}\right) \tag{3.6}$$

and

$$C_{**} = 2\cos^2(\lambda_1/2) + \lambda_1/2\sin(\lambda_1/2) - C_*\cos(\lambda_1). \tag{3.7}$$

The method of separation of variable is applied for finding the solution of the sub-problem (II) and finally we get the solution in the form

$$\tilde{R}_0 = C_1 \sin(\pi\tilde{z})\cos(\pi\tilde{y}), \tag{3.8}$$

where

$$C_1 = -\widetilde{R}_{\max} - \frac{\lambda_* L}{\pi^4}\left[\frac{1}{2}C_*\left(\frac{1+3\cos^2(\lambda_1/2)}{\cos\lambda_1/2}\right) - \frac{\lambda_1}{4}\sin\lambda_1/2\right]. \tag{3.9}$$

Therefore, the final model of vertical velocity component can be expressed as:

$$\begin{aligned}\tilde{r} &= C_1\sin(\pi\tilde{z})\cos(\pi\tilde{y}) + \lambda_*\frac{L}{\pi^4}\cos(\pi\tilde{y}) \\ &\times\left[\cos(\lambda_1\tilde{z}) - C_{**}\frac{\sin(\lambda_1\tilde{z})}{\sin\lambda_1} + \tilde{z}\left[C_*\cos(\lambda_1\tilde{z}) + \frac{\lambda_1}{2}\sin(\lambda_1\tilde{z})\right] + (2\tilde{z}-1)\right].\end{aligned} \tag{3.10}$$

The transverse component $\tilde{q}(\tilde{y},\tilde{z})$ of the secondary flow can be consequently expressed in the form of the continuity equation as (see Appendix for detailed solution),

$$\begin{aligned}\tilde{q} = -C_1\cos(\pi\tilde{z})\sin(\pi\tilde{y}) &- \frac{\lambda_* L\sin(\pi\tilde{y})}{\pi^5}\left[-\lambda_1\sin(\lambda_1\tilde{z}) - \frac{\lambda_1\cos(\lambda_1\tilde{z})}{\sin\lambda_1}C_{**}\right. \\ &+ \tilde{z}\left[-\lambda_1\sin(\lambda_1\tilde{z})C_* + \frac{\lambda_1^2}{2}\cos(\lambda_1\tilde{z})\right] \\ &\left.+ \left[C_*\cos(\lambda_1\tilde{z}) + \frac{\lambda_1}{2}\sin(\lambda_1\tilde{z})\right] + 2\right].\end{aligned} \tag{3.11}$$

Equations (3.10) and (3.11) represent the proposed models for secondary flow velocity components in straight rectangular shaped wide open channels.

4. Models under different bed structures

4.1. Non-elevated alternate rough and smooth bed strips of equal length

WANG and CHENG [5] proposed that the roughness of the beds changes without bed elevation in the secondary currents being generated. They showed this phenomenon in their empirical experiment named case S75. The study also

reported that when the bed strips are equal and smooth then secondary current cells make symmetrical shapes throughout the channel. They also reported that the shapes of the secondary current cells are in the counter-rotating cellular whose center is at $\tilde{z} = 0.5$. These secondary current cells have vertical dimensions of the flow depth and transverse dimensions of the mean bed width λ. It also showed that the streamlines that appeared in the result as a circle-like closed structure in the cross-sectional plane due to the continuity condition. In this study the Eq. (3.10) and (3.11) provides the model for the case S75 as follows:

$$\begin{aligned}\tilde{r} = {} & C_1 \sin(\pi\tilde{z})\cos(\pi\tilde{y}) \\ & + \lambda_* \frac{L}{\pi^4}\cos(\pi\tilde{y})\Bigg[\cos(\lambda_1\tilde{z}) - C_{**}\frac{\sin(\lambda_1\tilde{z})}{\sin\lambda_1} \\ & + \tilde{z}\Bigg[C_*\cos(\lambda_1\tilde{z}) + \frac{\lambda_1}{2}\sin(\lambda_1\tilde{z})\Bigg] + (2\tilde{z}-1)\Bigg]\end{aligned} \tag{4.1}$$

and

$$\begin{aligned}\tilde{q} = {} & -C_1\cos(\pi\tilde{z})\sin(\pi\tilde{y}) \\ & - \frac{\lambda_* L\sin(\pi\tilde{y})}{\pi^5}\Bigg[-\lambda_1\sin(\lambda_1\tilde{z}) - \frac{\lambda_1\cos(\lambda_1\tilde{z})}{\sin\lambda_1}C_{**} \\ & + \tilde{z}\Bigg[-\lambda_1\sin(\lambda_1\tilde{z})C_* + \frac{\lambda_1^2}{2}\cos(\lambda_1\tilde{z})\Bigg] \\ & + \Bigg[C_*\cos(\lambda_1\tilde{z}) + \frac{\lambda_1}{2}\sin(\lambda_1\tilde{z})\Bigg] + 2\Bigg].\end{aligned} \tag{4.2}$$

These equations give more general forms of the secondary flow velocity profile rather than assuming it empirically [5].

Finally, from the above equation we can find the stream function defined in the form as:

$$\tilde{\psi} = \int \overline{\tilde{r}}\, d\tilde{y}. \tag{4.3}$$

Here $\overline{\tilde{r}}$ denotes the non-dimensional secondary velocity in the perpendicular direction using $R_{\max}$. The stream function which is applicable in the cross-section for the symmetric secondary flow can be expressed in the following manner,

$$\begin{aligned}\tilde{\psi} = {} & \frac{\ell}{\pi}C_1\sin(\pi\tilde{z})\sin(\pi\tilde{y}) + \frac{\ell L\lambda_*}{\pi^5}\sin(\pi\tilde{y})\Bigg[\cos(\lambda_1\tilde{z}) - C_{**}\frac{\sin(\lambda_1\tilde{z})}{\sin\lambda_1} \\ & + \tilde{z}\Bigg[C_*\cos(\lambda_1\tilde{z}) + \frac{\lambda_1}{2}\sin(\lambda_1\tilde{z})\Bigg] + (2\tilde{z}-1)\Bigg],\end{aligned} \tag{4.4}$$

where $\ell = \bar{u}_*/R_{\max}$.

4.2. Non-elevated and alternate rough and smooth bed strips of unequal length

The transverse velocity profile $\tilde{r}$ proposed by [5] is wavelike with distinguished lengths along the spatial direction which indicates the up-flow and the down-flow zones. STUDERUS [33] and WANG and CHENG [5] reported that the maximum cross-sectional flow occurs over the interface of even and uneven bed strips also with the center of circulation. As a result, the uneven strip length is bigger than the even bed strip length and the flow cell becomes laterally skewed. WANG and CHENG [5] reported that for these cases the simple sine function $\sin \pi\tilde{y}$ is not applicable due to cell skewness. Hence, they propose a modified sine function as in the following form of $PS(\tilde{y})$ which is defined by a sinusoidal function that can count for the sidewise shift of the center of circulation and expressed as [5]:

$$PS(\tilde{y}) = \begin{cases} \frac{\lambda_{up}}{\lambda} \sin\left[\frac{(\tilde{y}-2m)\lambda}{\lambda_{dn}}\pi\right]; & 2m - \frac{\lambda_{dn}}{2\lambda} \le \tilde{y} \le 2m + \frac{\lambda_{dn}}{2\lambda}, \\ \frac{\lambda_{up}}{\lambda} \sin\left[\frac{\left(\tilde{y}-2m-\frac{\lambda_{dn}}{2\lambda}\right)}{\lambda_{up}}\pi + \frac{\pi}{2}\right]; & 2m + \frac{\lambda_{dn}}{2\lambda} \le \tilde{y} \le 2m + \frac{\lambda_{dn}}{2\lambda} + \frac{\lambda_{up}}{2\lambda}. \end{cases} \tag{4.5}$$

Hence the modified stream function can be expressed as:

$$\tilde{\psi} = \frac{\ell}{\pi} C_1 \sin(\pi\tilde{z}) PS(\tilde{y}) + \frac{\ell L \lambda_*}{\pi^5} PS(\tilde{y}) \Bigg[\cos(\lambda_1\tilde{z}) - C_{**}\frac{\sin(\lambda_1\tilde{z})}{\sin\lambda_1} + \tilde{z}\left[C_* \cos(\lambda_1\tilde{z}) + \frac{\lambda_1}{2}\sin(\lambda_1\tilde{z})\right] + (2\tilde{z}-1)\Bigg], \tag{4.6}$$

where $m = 0, \pm1, \pm2, \ldots$; $\lambda_{dn}, \lambda_{up}$ are span of the down-flow and up-flow regions over a water column, respectively; and λ is the averaged strip width of λ_{up} and λ_{dn}. This function can also be used for consistent bed conditions. After differentiating the stream function, the secondary velocity components can be obtained as:

$$\tilde{r} = C_1 \sin(\pi\tilde{z}) PC(\tilde{y}) + \lambda_* \frac{L}{\pi^4} PC(\tilde{y}) \Bigg[\cos(\lambda_1\tilde{z}) - C_{**}\frac{\sin(\lambda_1\tilde{z})}{\sin\lambda_1} + \tilde{z}\left[C_* \cos(\lambda_1\tilde{z}) + \frac{\lambda_1}{2}\sin(\lambda_1\tilde{z})\right] + (2\tilde{z}-1)\Bigg] \tag{4.7}$$

and

$$\tilde{q} = -C_1 \cos(\pi\tilde{z}) PS(\tilde{y}) - \frac{\lambda_* L PS(\tilde{y})}{\pi^5}\Bigg[-\lambda_1 \sin(\lambda_1\tilde{z}) - \frac{\lambda_1\cos(\lambda_1\tilde{z})}{\sin\lambda_1} C_{**} + \tilde{z}\left[-\lambda_1 \sin(\lambda_1\tilde{z}) C_* + \frac{\lambda_1^2}{2}\cos(\lambda_1\tilde{z})\right] + \left[C_* \cos(\lambda_1\tilde{z}) + \frac{\lambda_1}{2}\sin(\lambda_1\tilde{z})\right] + 2\Bigg], \tag{4.8}$$

where $PC(\tilde{y})$ is the derivative of the $PS(\tilde{y})$ function. The sidewise shift of the center of circulation is captured through the functions PS and PC. It is also noted that the models of Eq. (4.7) and (4.8) are more general than the proposed model of WANG and CHENG [5] and previous models of [26] and [27].

4.3. Elevated alternate rough and smooth bed-forms

For the above two cases, the cellular secondary current cells are induced only on the lateral variation in the bed roughness. The experimental results of [5] for the case WR showed that the cellular form of the secondary current is generated by the wavy ridges without the transverse roughness variations. Although different bed configurations are present in the natural resources, the structures of the secondary cells are very similar. The similarity of the cells has implied that the bed trough for the case WR could serve similarly to the rough strips of the beds. The lateral gradient of bed shear stress is caused by the lateral bed perturbation either in bed roughness or the elevation of the bed. The local bed shear stress may increase at the location of relatively deeper flow depth or larger roughness. This is the phenomenon that leads to the down flow occurring just over the rough strips or troughs and up flow occurs over smooth strips or ridges. We extend our study further in the way that the previously proposed stream function to the wavy bed surface by introducing the vertical coordinate system in the following transformation,

$$\tilde{z} = \tilde{z} - b\left(\frac{y}{h}\right), \tag{4.9}$$

where $b\,(\tilde{y})$ is the bed function corresponding to the vertical coordinate. The following elevated bed functions are considered:

$$b(\tilde{y}) = \frac{A}{\lambda^2}\tilde{y}^2 \qquad \text{(Case WR)}, \tag{4.10}$$

where A is taken as a constant that is related to the bed elevation. For simplicity of the solution $\tilde{z} - \frac{b(\tilde{y})}{h} = \tilde{z}'$ is substituted. Therefore, the stream function for the wavy ridges can be written in the form below:

$$\tilde{\psi}(\tilde{y},\tilde{z}') = \left[\frac{\ell}{\pi}C_1\sin(\pi\tilde{z}') + \frac{\ell L\lambda_*}{\pi^5}\left[\cos(\lambda_1\tilde{z}') - C_{**}\frac{\sin(\lambda_1\tilde{z}')}{\sin\lambda_1}\right.\right. \tag{4.11}$$
$$\left.\left. + \tilde{z}'\left[C_*\cos(\lambda_1\tilde{z}') + \frac{\lambda_1}{2}\sin(\lambda_1\tilde{z}')\right] + (2\tilde{z}'-1)\right]\right]PS(\tilde{y}).$$

Consequently the secondary velocity components are obtained as:

$$\tilde{r} = PC(\tilde{y})\left[\frac{1}{\pi}C_1\sin(\pi\tilde{z}')\right. \tag{4.12}$$
$$+\frac{L\lambda_*}{\pi^5}\left\{\cos(\lambda_1\tilde{z}')-C_{**}\frac{\sin(\lambda_1\tilde{z}')}{\sin\lambda_1}+\tilde{z}'\left(C_*\cos(\lambda_1\tilde{z}')+\frac{\lambda_1}{2}\sin(\lambda_1\tilde{z}')\right)+(2\tilde{z}'-1)\right\}\Bigg]$$
$$-PS(\tilde{y})\frac{\partial b(\tilde{y})}{\partial\tilde{y}}\left[C_1\cos(\pi\tilde{z}')+\frac{L\lambda_*}{\pi^5}\left[-\lambda_1\sin(\lambda_1\tilde{z}')-\frac{C_{**}\lambda_1}{\sin\lambda_1}\cos(\lambda_1\tilde{z}')\right.\right.$$
$$\left.\left.+C_*\cos(\lambda_1\tilde{z}')+\frac{\lambda_1}{2}\sin(\lambda_1\tilde{z}')+\tilde{z}'\left\{-C_*\lambda_1\sin(\lambda_1\tilde{z}')+\frac{\lambda_1^2}{2}\cos(\lambda_1\tilde{z}')\right\}+2\right]\right]$$

and

$$\tilde{q} = -C_1\cos(\pi\tilde{z}')PS(\tilde{y})-\frac{\lambda_* LPS(\tilde{y})}{\pi^5}\left[-\lambda_1\sin(\lambda_1\tilde{z}')-\frac{\lambda_1\cos(\lambda_1\tilde{z}')}{\sin\lambda_1}C_{**}\right. \tag{4.13}$$
$$\left.+\tilde{z}'\left[-\lambda_1\sin(\lambda_1\tilde{z}')C_*+\frac{\lambda_1^2}{2}\cos(\lambda_1\tilde{z}')\right]+\left[C_*\cos(\lambda_1\tilde{z}')+\frac{\lambda_1}{2}\sin(\lambda_1\tilde{z}')\right]+2\right].$$

Figures 7 and 8 represent the velocity profiles of $\tilde{r}$ and $\tilde{q}$ for the case WR. We have considered the bed functions in the following forms and substituted those into Eq. (4.11). In Fig. 10 these studies showed the contour profiles of the stream function with different kinds of bed configurations.

$$b_2(\tilde{y}) = \frac{A}{\lambda^3}(2+\tilde{y}^2), \tag{4.14}$$

$$b_3(\tilde{y}) = \frac{A}{\lambda^3}(2-\tilde{y}^2), \tag{4.15}$$

$$b_4(\tilde{y}) = \begin{cases} -\frac{A}{\lambda^3}\tilde{y} & \text{if } -1 \le \tilde{y} < 0, \\ \frac{A}{\lambda^3}\tilde{y} & \text{if } 0 < \tilde{y} \le 1, \end{cases} \tag{4.16}$$

$$b_5(\tilde{y}) = \begin{cases} \frac{A}{\lambda^3}(1+\tilde{y}) & \text{if } -1 \le \tilde{y} < 0, \\ \frac{A}{\lambda^3}(1-\tilde{y}) & \text{if } 0 < \tilde{y} \le 1. \end{cases} \tag{4.17}$$

In Fig. 10 the contour profile of the stream function with respect to the different bed formations is shown by substituting Eqs. (4.14)–(4.17) in to Eq. (4.11).

5. Comparison and validation with experimentally observed data

In this part, the proposed velocity models of secondary flow velocity components along the perpendicular and transverse direction and derived stream functions are validated with the experimentally observed data. WANG and CHENG [5]

performed experiments along a wide open channel with the effects of bed perturbation to generate secondary currents. Since in the present study, the theoretical assumptions are similar to that and the effects of the sidewall are absent, this experimental data is employed for validation. WANG and CHENG [5] performed the experiments in a wide pen channel changing bed-roughness and considering different bed-forms in a straight rectangular wide open channel which was 14 m long, 0.6 m wide. For experiments S75 and S50 two different types of bed strips were used. In both cases, the bed was developed with alternative smooth and rough bed strips. The rough bed strips were made of the uniform sediment particle diameter of the mean diameter of 2.55 mm and densely packed such that no particles were not able to move. leave from the bed surface. Apart from these two cases, run WR was performed with wavy ridges where a bed height changes with lateral y-coordinates. The channel slope for test Cases S75 and S50 was 0.0012 and for the test Case WR, 0.001 and the Reynolds number were kept at 44,206 and 38,684 respectively for these test cases. The high Reynolds number indicates that the secondary current occurs in a turbulent flow and is generated due to bed effects. The obtained validation results are discussed below.

Figures 2, 4 and 7 show the attestation of the proposed contour profiles of the secondary velocity components (i.e. Eqs. (4.1), (4.2), (4.7), (4.8), (4.12) and (4.13)) for various longitudinal bed strips and wavy bed ridges. In Figs. 2 and 4 the contour of both the velocity components along perpendicular and transverse directions for the equal and unequal rough and smooth bed strips are plotted. In these figures, the dimensionless velocities $r/R_{\max}$ and $q/R_{\max}$ are plotted against the coordinates $\tilde{y}$ and $\tilde{z}$. The value of $R_{\max}$ is taken 2% of the mean velocity U_m for the case of S75 and 2.5% for the case of S50 (taken from the experimental observations of [5]). Here the mean velocity is calculated from the below equation

$$U_m = \int_{\tilde{z}_0}^{1} \left[\frac{u_*}{\kappa} \ln\left(\frac{\tilde{z}}{\tilde{z}_0}\right) - \frac{2\Pi u_*}{\kappa} \cos^2\left(\frac{\pi \tilde{z}}{2}\right) + U_{\max} \right] d\tilde{z}, \tag{5.1}$$

where $\tilde{z}_0 = z_0/h$ and z_0 denotes the zero primary velocity level. The parameter λ_* denotes the bed perturbation parameter and is computed from the experimental data. The values of other parameters (indicated in the figure caption) are taken from the experimental data. To compare the present result, the empirical model of [5] is also plotted in these figures. From this figure, it can be seen that similar results are achieved in all the test Cases of S75, S50, and WR. Further, it can be seen from Figs. 2 and 4 that zero vertical velocity (i.e. component r) occurs at $y/\lambda = -0.5$ for the case S75; whereas it shifts to the location $y/\lambda = -0.666$ for test case S50. This occurs due to the change in the length of bed strips. It is found from the experimental observation that vertical velocity vanishes at the

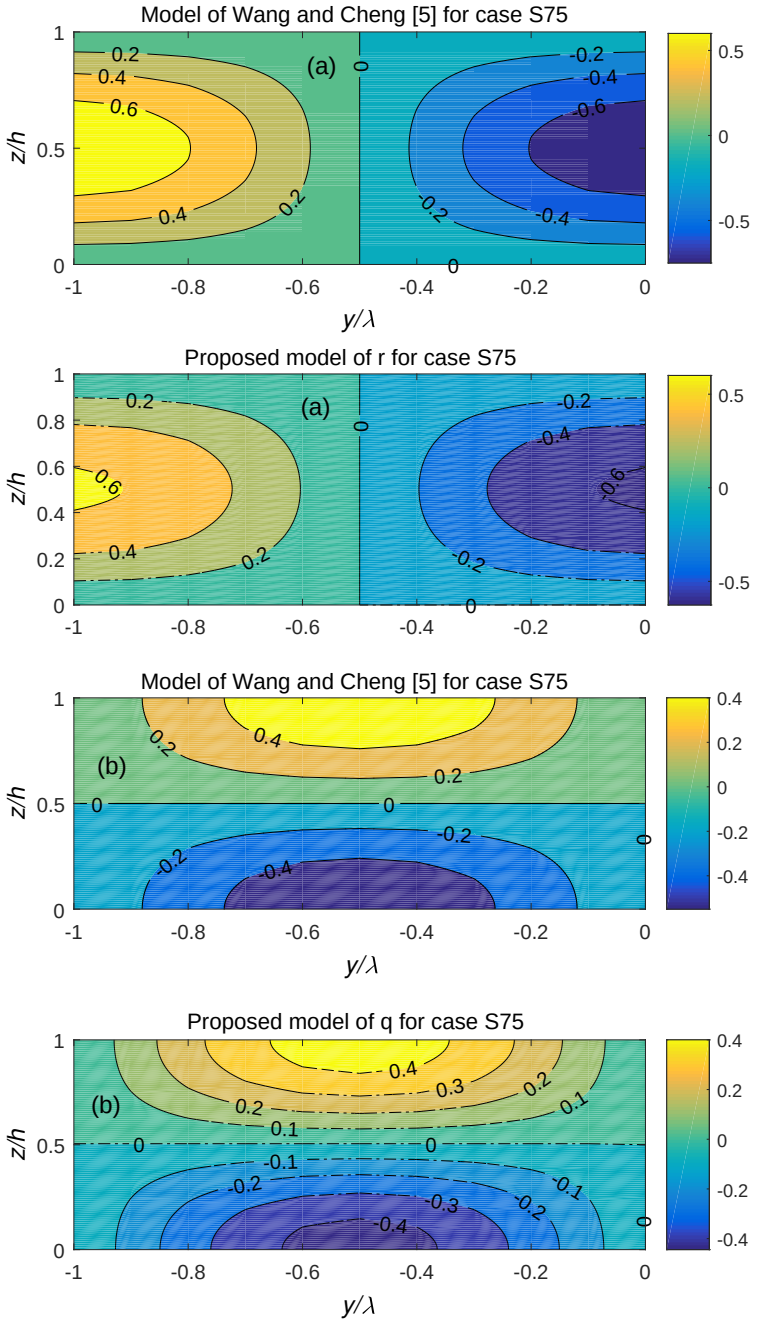

FIG. 2. The contour profiles of subsisting model of [5] (case S75) and (a) Eq. (3.10) and (b) Eq. (3.11) for the symmetrical flow cells are being compared. The velocities r and q are made dimensionless by $0.02U_m$ and the values on the contour lines indicate the dimensionless velocities. The values of parameters being taken as $\alpha = 0.2$, $\tilde{z}_0 = 6 \times 10^{-4}$, $R_{\max} = 0.0094\,\mathrm{m/s}$, $h = 0.075\,\mathrm{m}$, $J_l = 0.0012$, $u_* = 0.03\,\mathrm{m/s}$, $B = 0.6\,\mathrm{m}$, $\lambda_* = -0.01$.

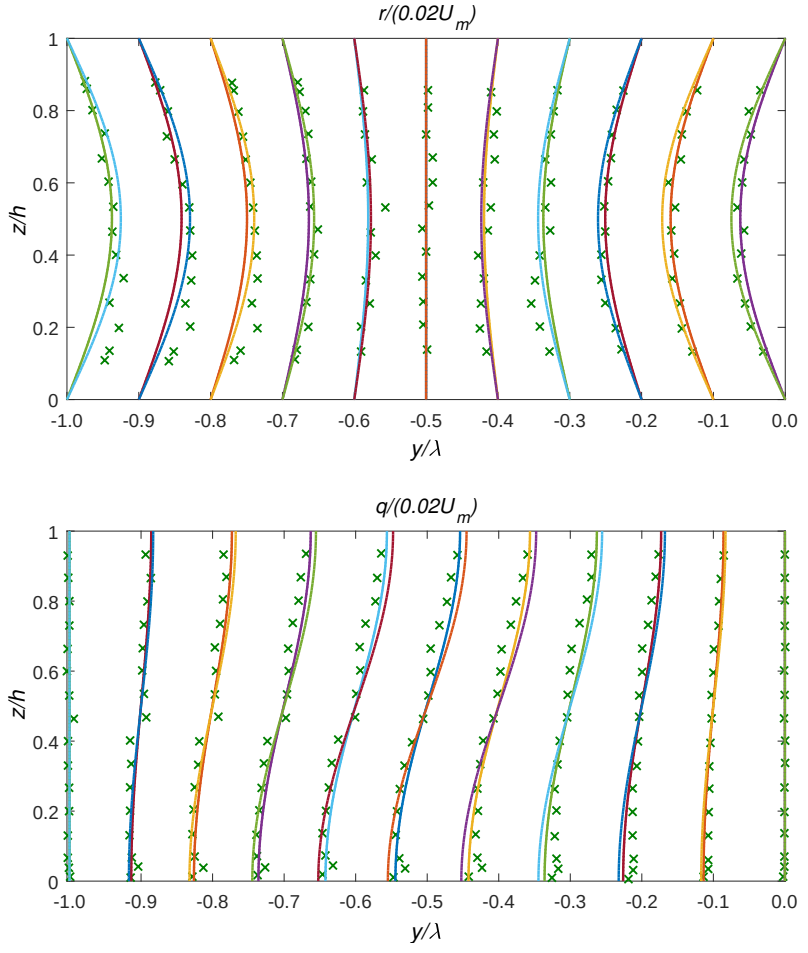

FIG. 3. The velocity profiles of $\tilde{r}/R_{\max}$ with Eq. (3.10) and $\tilde{q}/R_{\max}$ with Eq. (3.11) are compared and validated with the subsisting model of [5] for symmetrical flow cells (case S75). The values * of parameters are taken as $\alpha = 0.2$, $\tilde{z}_0 = 6 \times 10^{-4}$, $\lambda_* = -0.01$, $R_{\max} = 0.0094\,\mathrm{m/s}$, $h = 0.075\,\mathrm{m}$, $J_l = 0.0012$, $u_* = 0.03\,\mathrm{m/s}$, $B = 0.6\,\mathrm{m}$. Here the dashed lines $(--)$ represent the model of [5], continuous lines $(-)$ represent the proposed model and cross symbols $(\times)$ indicate the experimental data points.

junction of smooth and rough bed strips. The shifting of the location of $\widetilde{r} = 0$, in these figures suggests that the proposed model correctly captures the flow field. Similarly, in these figures it can be observed that a symmetrical flow field is present for the case S75, where $\lambda_{dn}/\lambda_{up}$ ratio is a unit (which corresponds to equal length bed strips); whereas when the bed strips length are not equal the flow field becomes horizontally distorted. The change of cellular-shaped cells occurs due to the bed effects. Since the effects of side walls are restricted to

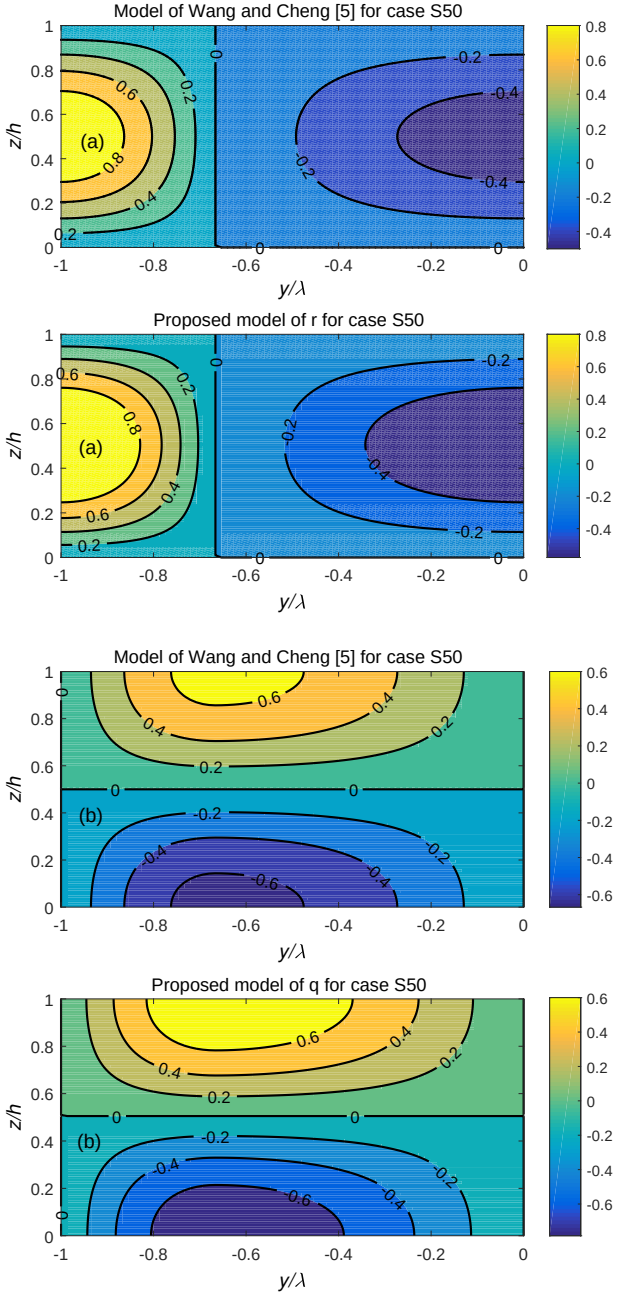

FIG. 4. The contour profiles of existing model of [5] (case 50) and (a) Eq. (4.7) and (b) Eq. (4.8) for the laterally skewed flow cells are being compared. The velocities r and q are made dimensionless by $0.025U_m$ and the values on the contour lines indicate the dimensionless velocities. The values of parameters being taken as $\alpha = 0.2$, $\tilde{z}_0 = 8 \times 10^{-4}$, $R_{\max} = 0.0104\,\mathrm{m/s}$, $h = 0.075\,\mathrm{m}$, $J_l = 0.001$, $u_* = 0.0271\,\mathrm{m/s}$, $B = 0.6\,\mathrm{m}$, $\lambda_* = -0.01$.

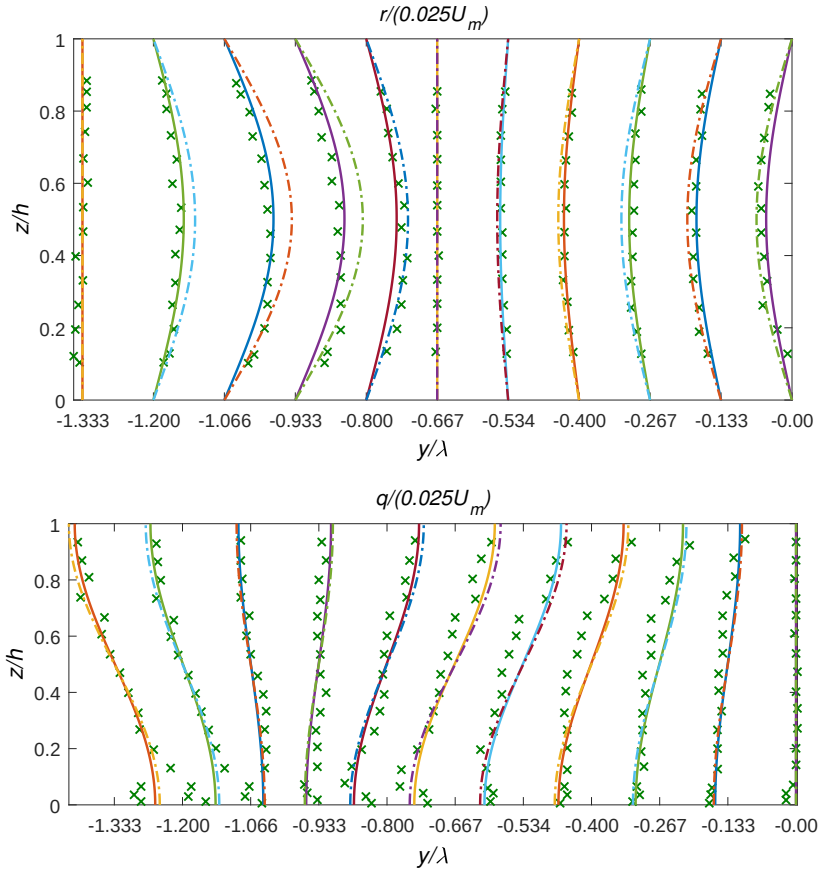

FIG. 5. The velocity profiles of $\tilde{r}/R_{\max}$ with Eq. (4.7) and $\tilde{q}/R_{\max}$ with Eq. (4.8) being compared and validated with the existing model of [5] for laterally skewed flow cells (case S50). The values of parameters being taken as $\alpha = 0.2$, $\tilde{z}_0 = 8 \times 10^{-4}$, $\lambda_* = -0.01$, $R_{\max} = 0.0104\,\mathrm{m/s}$, $h = 0.075\,\mathrm{m}$, $J_l = 0.001$, $u_* = 0.0271\,\mathrm{m/s}$, $B = 0.6\,\mathrm{m}$. Here the dashed lines (−−) represent the model of [5], continuous lines (−) represents the proposed model and cross symbols (×) indicate the experimental data points.

a maximum of three times the flow depth near the sidewall region, it can be considered that flow in the central section is related to the bed strips. In the case of equal lengths $\lambda_{up} = \lambda_{dn}$, the center of circulation appears at the junction of these two lengths, and upflow and downflow zones have the same lengths and as a consequence cellular patterns are formed. When the length of the smooth strip or λ_{dn} is decreased and the length of the rough strip or λ_{up} increases, the region of upflow is compressed and the region of downflow is elongated. Thus, the circular shape is distorted and as a result, laterally skewed cells are formed. Whereas different observation is found in the case WR in Fig. 7. In this case, flow cells become vertically distorted. This occurs, as the local bed height

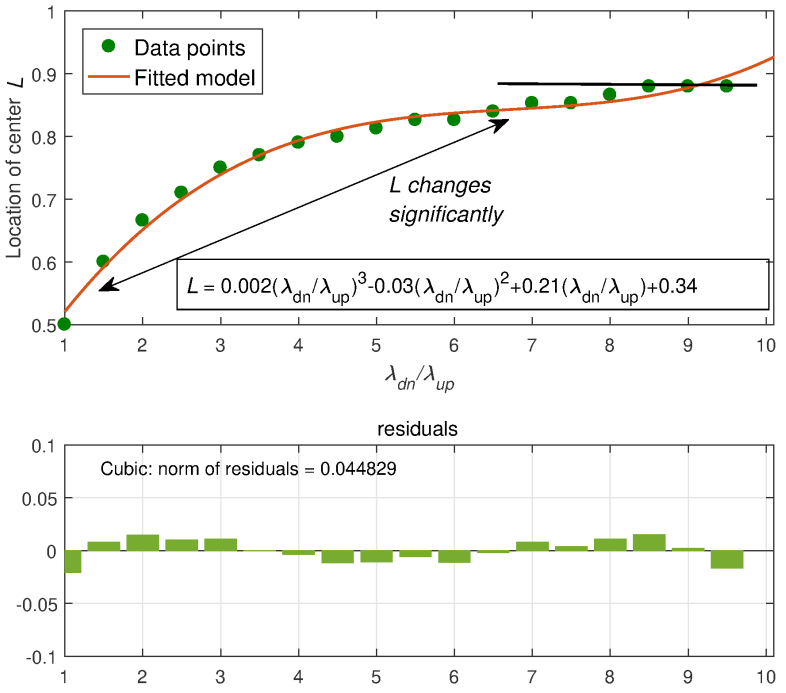

FIG. 6. Change of circulation center with the ratio $\lambda_{dn}/\lambda_{up}$.

changes along the lateral direction, and the circular shape deforms according to the bedforms. These results suggest that the flow field or in particular the secondary current field changes with bed perturbation. This result is consistent with the experimental findings.

Figure 3 gives the validation result of the proposed model (Eqs. (3.10) and (3.11)) with experimentally observed data for the case of S75 i.e. equal and alternative rough and smooth bed strips. In this case, circular symmetric flow cells are observed. The values of the parameters are indicated in the figures which are calculated in a similar way as aforementioned. It can be seen from the picture that the vertical $\widetilde{r}$ profile is symmetrical about $y/\lambda = -0.5$. In the region, $-1.0 \leq \widetilde{y} \leq -0.5$ vertical velocity is positive which corresponds to the upward flow and in the region, $-0.5 \leq \widetilde{y} \leq 0$, vertical velocity shows negative which occurs due to the downward flow. Similarly, lateral velocity is zero at $y/\lambda = 0.0$ (central section) and -1.0 (midpoint of smooth strips) as observed in Fig. 3. The reason can be explained as follows. The vertical velocity is downward at the central section when $y/\lambda = 0$ and upward at $y/\lambda = -1$. Therefore in these two sections, only vertical velocity exists and transverse velocity shows a zero value. In the section $y/\lambda = -0.5$, only transverse current exists as a result vertical velocity appears as zero. The results show that the present study improves the

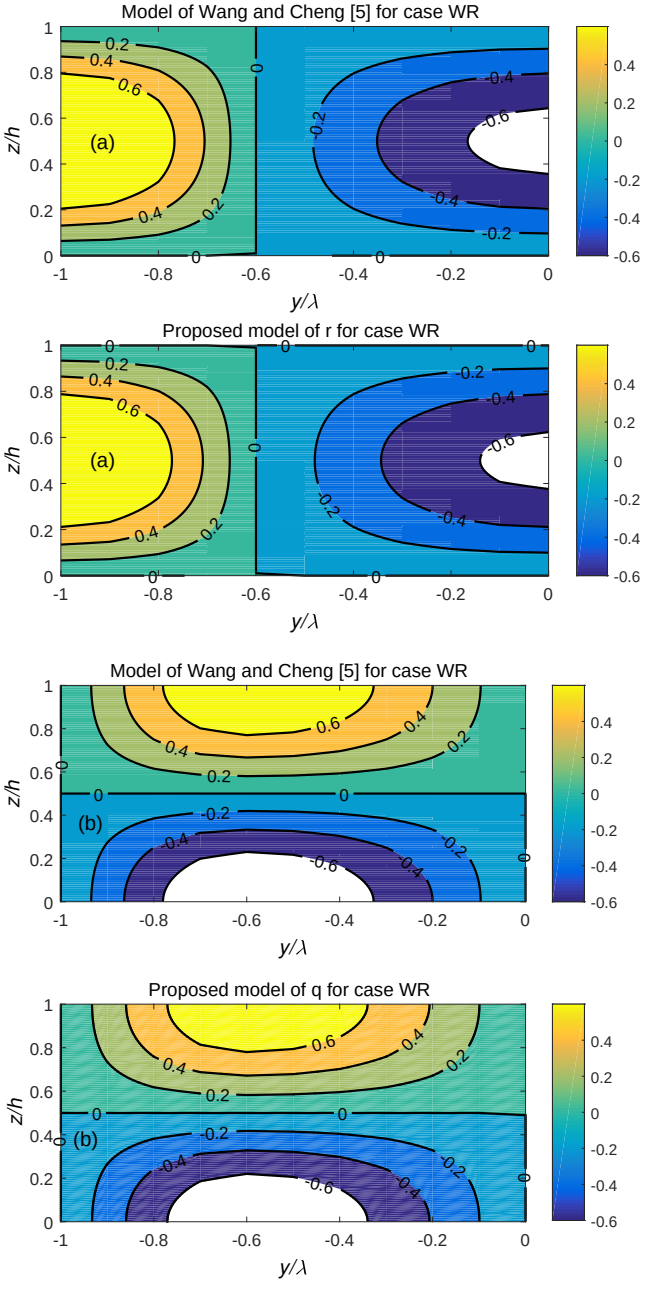

FIG. 7. The contour profiles of existing model of [5] (case WR) and the (a) Eq. (4.12) and (b) Eq. (4.13) for the vertically distorted flow cells are compared. The velocities r and q are made dimensionless by $0.016U_m$ and the values on the contour lines indicate the dimensionless velocities. The values of parameters are taken as $\alpha = 0.2$, $\tilde{z}_0 = 3 \times 10^{-4}$, $R_{\max} = 0.007\,\mathrm{m/s}$, $h = 0.075\,\mathrm{m}$, $J_l = 0.008$, $u_* = 0.0243\,\mathrm{m/s}$, $B = 0.6\,\mathrm{m}$, $\lambda_* = 0.002$.

previous prediction. To quantify the improvement result, the root mean squared error (RMSE) is computed as

$$RMSE = \sqrt{\frac{1}{N}\sum_{i=1}^{N}(v_{i(cp)} - v_{i(ob)})^2}, \tag{5.2}$$

where N denotes the total number of data points, $v_{i(cp)}$ denotes the computed velocity and $v_{i(ob)}$ is the observed velocity at i^{th} data point. Computed RMSE errors are presented in Table 2 where $RMSE_{pm}$ and $RMSE_{wc}$ indicate the error corresponding to the preset model and the model of [13]. It can be found that in most of the cases, a minimum error corresponds to the present model. This suggests the improvement in the predicted result. It can be noted that lateral velocity deviates near the region of $y/\lambda = -0.5$. This may be due to the sudden change in bed roughness which can be removed with some suitable values of the bed perturbation parameter.

Similarly, the vertical and transverse velocity components are plotted for the case S50 (i.e. laterally skewed secondary flow cells as can be observed from Fig. 4) are explained in Fig. 5. Here the velocity is made dimensionless by considering 2.5% of the mean velocity value U_m as suggested in [5] and the equations are plotted against the vertical line z/h at the different sections with y/λ from -1.3333 to 0.0. The model of [5] is also plotted due to comparison purposes only. In the figure, continuous lines denote the present model and dash-dotted lines indicate the model of Wang and Cheng. The conditions of the flow and other parameters are taken from the experimentally observed data of [5]. In both of these cases of velocity, the present model suggests better prediction of the data points. It can be seen that in the region $-1.333 \leq \widetilde{y} \leq -0.667$, both the velocity profile significantly changes due to the increase in length of a rough bed strip with $\lambda_{dn}/\lambda_{up} = 2$. The model can also predict this horizontal distortion well. The experiments of [5] only tell us about the flow field for two values of the ratio $\lambda_{dn}/\lambda_{up}$ equal to one and two. We have investigated further other possible values of this ratio. We observed that with the change in the secondary flow field (horizontal distortion), the center of circulation gradually shifts. The change of circulation with different values of the ratio $\lambda_{dn}/\lambda_{up}$ is plotted in Fig. 6. It is observed from the result that the circulation center does not shift linearly with the ratio whereas it follows a cubic relation. A least square analysis shows that the center shifts along the curve, it is given as:

$$\text{Location of center } L = 0.002\left(\frac{\lambda_{dn}}{\lambda_{up}}\right)^3 - 0.03\left(\frac{\lambda_{dn}}{\lambda_{up}}\right)^2 + 0.21\left(\frac{\lambda_{dn}}{\lambda_{up}}\right) + 0.34. \tag{5.3}$$

In the figure, the residual norm is also plotted which has the value 0.044829. In the analysis, it is found that the location L significantly changes from 0.5 to 0.87

TABLE 2. Error analysis between proposed models in Eqs. (4.1), (4.2), (4.7), (4.8), (4.12) and (4.13) and model of [13] using root mean squared error analysis method (here * indicates minimum error value).

	$\tilde{r}$		$\tilde{q}$	
y/λ	$RMSE_{pm}$	$RMSE_{wc}$	$RMSE_{pm}$	$RMSE_{wc}$
Case S75 (Symmetrical Flow cells)				
−1.0	0.1994	0.1774*	0.0284	0.0284
−0.9	0.1919	0.1458*	0.0284*	0.0771
−0.8	0.1832	0.1274*	0.0907*	0.1164
−0.7	0.0903	0.0507*	0.0974*	0.1333
−0.6	0.0885	0.0723*	0.1091*	0.1496
−0.5	0.0511	0.0511	0.0998*	0.1549
−0.4	0.0897*	0.0968	0.1103*	0.1788
−0.3	0.1276	0.1203*	0.1223*	0.1880
−0.2	0.0694	0.0634*	0.1023*	0.1513
−0.1	0.0521*	0.1040	0.0462*	0.0699
0.0	0.0790*	0.0837	0.0103	0.0103
Case S50 (Laterally skewed Flow cells)				
−1.3333	0.0182	0.0182	0.0097*	0.0350
−1.2000	0.0086*	0.0129	0.0225*	0.0429
−1.066	0.0284*	0.0357	0.0.0097*	0.0175
−0.933	0.0059*	0.0128	0.0401*	0.0479
−0.800	0.0049	0.0004*	0.0148*	0.0353
−0.667	0.0001	0.0001	0.0108*	0.0361
−0.534	0.0026*	0.0041	0.0329	0.0088*
−0.400	0.0017	0.0011*	0.0382	0.0178*
−0.267	0.007	0.0043*	0.0327	0.0180*
−0.133	0.0325	0.0280*	0.0227	0.0148*
0.0	0.0425	0.0377*	0.0001	0.0001
Case WR (Vertically distorted Flow cells)				
−1.0	0.0176*	0.0180	0.0094	0.0094
−0.9	0.0172	0.0167*	0.0096*	0.0352
−0.8	0.0148	0.0144*	0.0369	0.0108*
−0.7	0.0011*	0.0014	0.0145*	0.0478
−0.6	0.0188	0.0188	0.0486	0.0187*
−0.5	0.0157*	0.0165	0.0543	0.0197*
−0.4	0.0216*	0.0235	0.0351	0.0230*
−0.3	0.0137*	0.0151	0.0327	0.0147*
−0.2	0.0238*	0.0254	0.0290	0.0047*
−0.1	0.0158*	0.0192	0.0129	0.0045*
0.0	0.0388*	0.0420	0.0046	0.0046

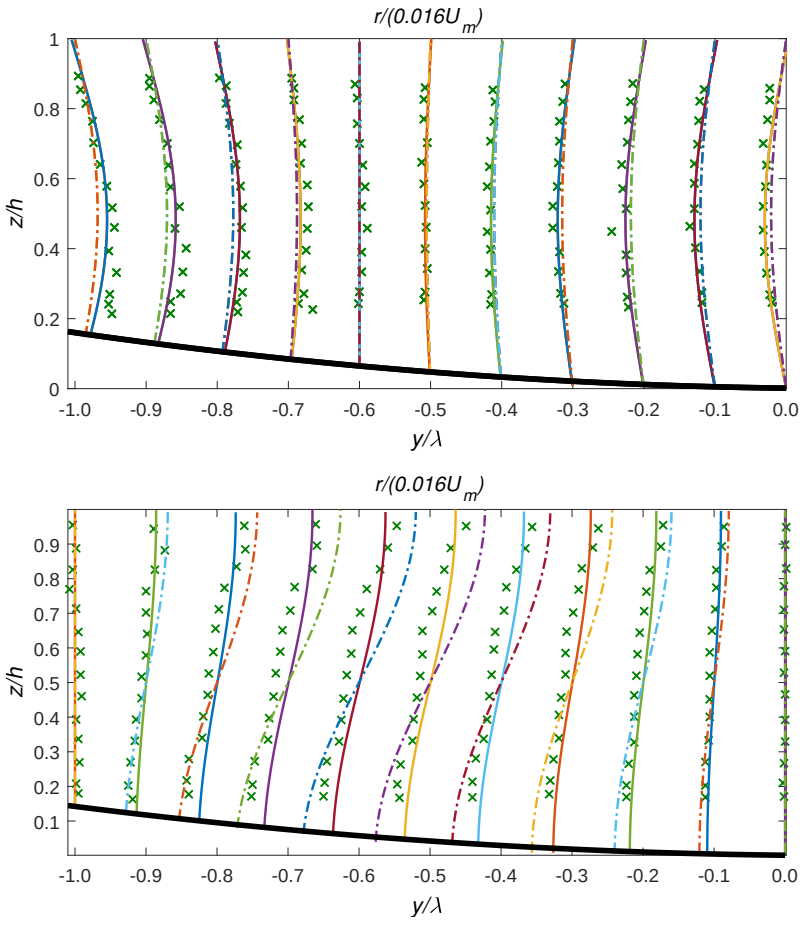

FIG. 8. The velocity profiles of $\tilde{r}/R_{\max}$ with Eq. (4.12) and $\tilde{q}/R_{\max}$ with Eq. (4.13) being compared and validated with the existing model of [5] for vertically distorted flow cells (case WR). The values of parameters being taken as $\alpha = 0.2$, $\tilde{z}_0 = 3 \times 10^{-4}$, $R_{\max} = 0.007\,\mathrm{m/s}$, $h = 0.075\,\mathrm{m}$, $J_l = 0.008$, $u_* = 0.0243\,\mathrm{m/s}$, $B = 0.6\,\mathrm{m}$, $\lambda_* = 0.002$. Here the dashed lines $(--)$ represent the model of [5], continuous lines $(-)$ represent the proposed model and cross symbols $(\times)$ indicate the experimental data points.

with $\left(\frac{\lambda_{dn}}{\lambda_{up}}\right)$ up to its value which is eight. Thereafter no change in L is obtained. This occurs since when the ratio further increases from eight, no change in bed configuration is present as the dimensionless width of the channel is 8.

Figure 8 shows the validation of proposed vertical and transverse velocity components for the case of WR i.e. wavy bedforms. In the figure velocity curves are plotted after making dimensionless by $0.016Um$ and the equations are plotted against the vertical line z/h at the different sections with y/λ ranging from -1.0 to 0.0. The model of [5] is also plotted due to comparison purposes only. The flow

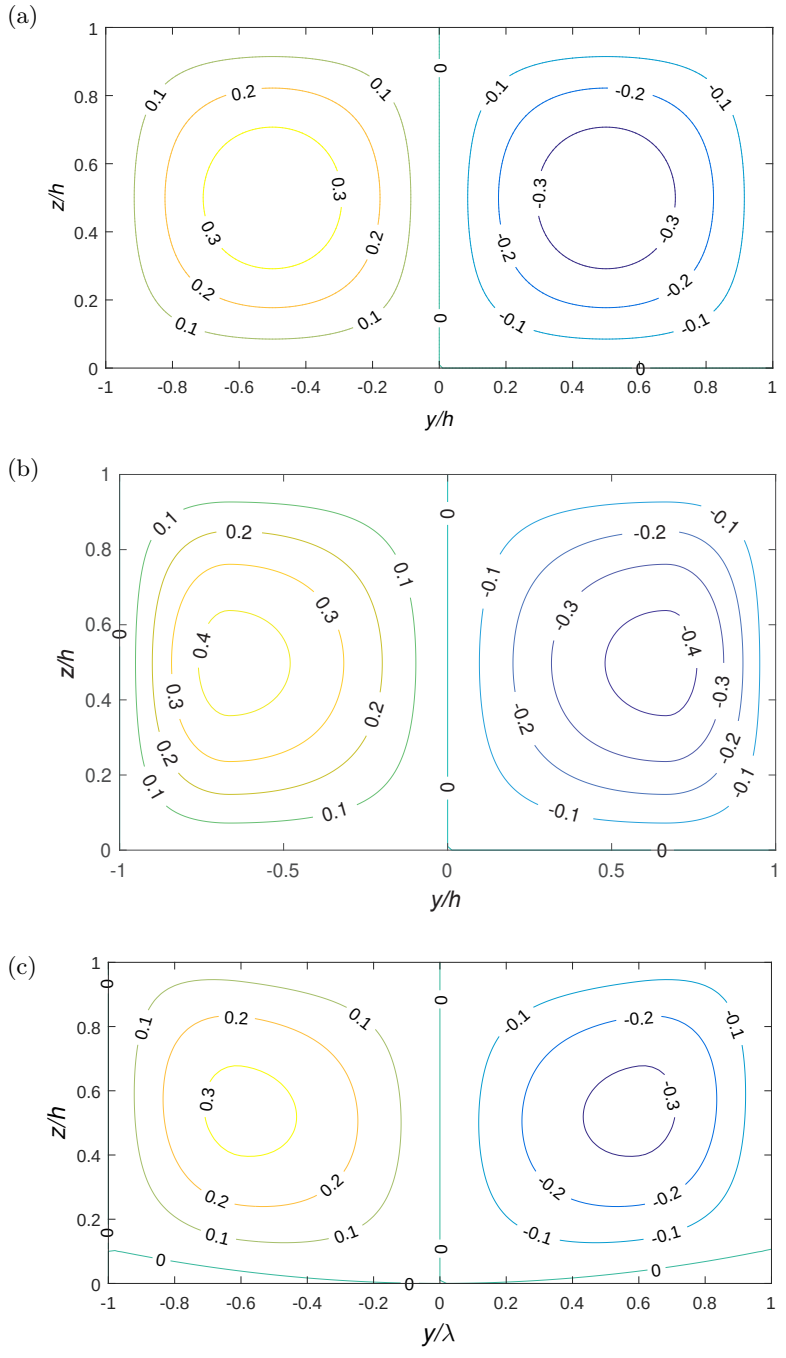

FIG. 9. Contour profile of different structures of secondary flow cells stream function of (a) Eq. (4.4) for the case S75, (b) Eq. (4.6) for the case S50, (c) Eq. (4.11) for the case WR. The closed curves are $\tilde{\psi}$ contours computed using the proposed models.

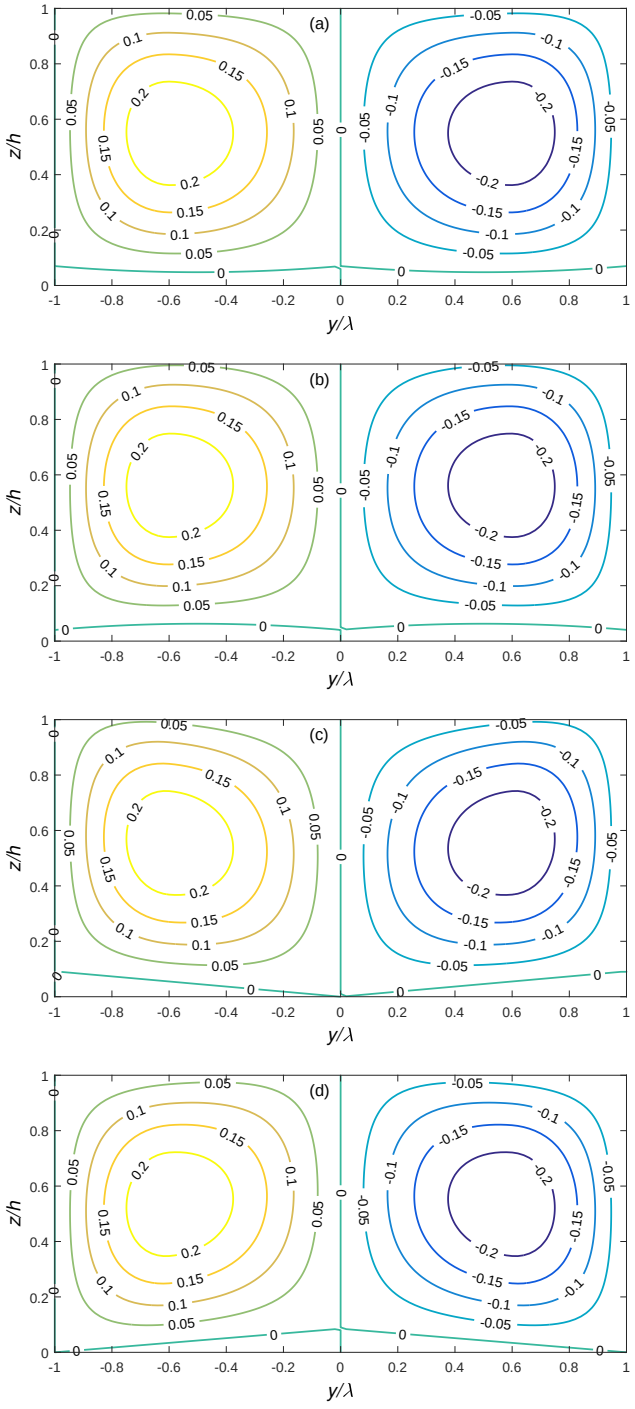

FIG. 10. Structure of secondary flow cells (from Eq. (4.11)) with various bed forms as shown in Eqs. (4.14)–(4.17) with various type of bed configuration.

conditions and other values of parameters are considered from the experimental data of [5]. In both of these cases of the vertical and transverse velocity profiles for elevated longitudinal bedforms, the proposed model gives more improved results than the model of [5].

Further in Figs. 9 and 10 streamlines for secondary flow cells are presented. Figure 9(a) shows the contour profile of the three Cases S75, S50, and WR that are considered in their experiments of [5]. It can be seen in this figure that the symmetric secondary flow cells (top figure; which are obtained from Eq. (4.4) with the corresponding conditions $h = 0.075\,\mathrm{m}$, $\lambda = 0.075\,\mathrm{m}$ and $R_{\max} = 0.02U_m$) occur for an equal length of both the smooth and rough bed strips; horizontally distorted flow cells (middle figure obtained from the Eq. (4.6)) occur due to increase in the length of rough bed strips and vertically distorted secondary cells (bottom figure obtained from Eq. (4.11)) occur for wavy elevated bedforms. These secondary flow cells are similar as reported in the experiments of [5]. In Fig. 10 the secondary flow cells are plotted for four other types of bedforms: upward concave and convex bed bumps and triangular-shaped bed forms (with two cases). This figure shows the further extension of the study for other different types of bedforms. It can be seen that for the bump-type beds, a laterally distorted profile is observed; whereas circular cells become vertically distorted for triangular bedforms. The vertically distorted case is obtained since the local bed height constantly increases/decreases throughout full closed circular contours. This result is also supported by the experimental results observed in [5] for the case of wavy ridges. Whereas in the case of bump-type bedforms, the bed slope does not increase/decrease consistently. In this case, vertical distortion is not present. Further, when the bump bed structure is convex, flat streamlines are observed at the maximum local bed height.

6. Discussion

This section discusses some general aspects of the nature of the considered boundary conditions. From the analysis of experimental data from [23–25] we have observed that the maximum velocity may not always occur at the middle of the channel. Therefore, we modify that condition. Also, due to the inadequacy of secondary velocity data at the free surface, new boundary conditions are being imposed by freeing the upper boundary conditions. From the above-mentioned data, since the position of the maximum velocity is different, L_* (constant) is taken which indicates the location of the maximum vertical velocity from the channel bottom. Starting from Eq. (3.4) and imposing the new boundary conditions as:

$$\tilde{r}|_{\tilde{z}=0} = 0, \quad \tilde{r}|_{|\tilde{y}|=1,\,\tilde{z}=L_*} = \widetilde{R}_{\max}, \quad \text{or} \quad \frac{\partial \tilde{r}}{\partial \tilde{z}}|_{\tilde{z}=L_*} = 0. \tag{6.1}$$

After considering these boundary condition the possible form of the vertical velocity component is obtained as:

$$\tilde{r} = C_1 \sin\left(\frac{\pi\tilde{z}}{2L_*}\right)\frac{\cos(1/2-\tilde{y}+\pi/2)\chi_1}{\sin\frac{\chi_1}{2}} + \lambda_*\frac{L}{\pi^4}\cos(\pi\tilde{y})\left[\cos(\lambda_1\tilde{z}) - C_{**}\frac{\sin(\lambda_1\tilde{z})}{\sin\lambda_1} + \tilde{z}\left[C_*\cos(\lambda_1\tilde{z}) + \frac{\lambda_1}{2}\sin(\lambda_1\tilde{z})\right] + (2\tilde{z}-1)\right], \tag{6.2}$$

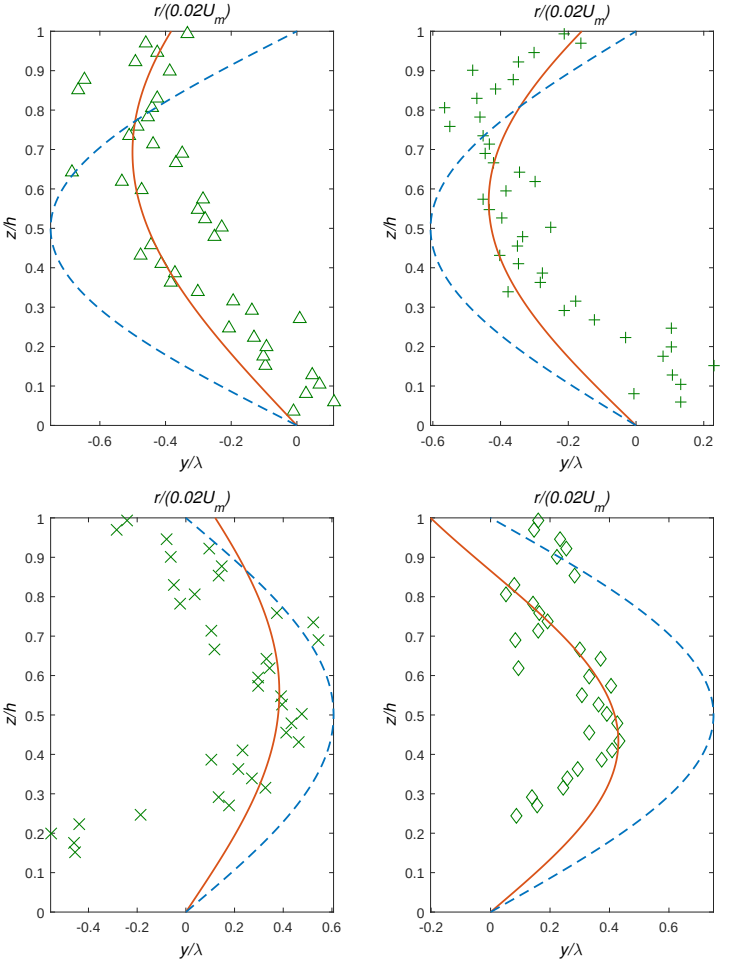

FIG. 11. Validation of the model Eq. 6.2 with experimental data of [23] and comparison with the model of [5]. Here continuous lines ('–') denote the present study, dashed lines ('– –') denote the model of [5] and symbols (⋄, ×, +, △) denote data points.

where

$$C_1 = -R_{\max} - \frac{L\lambda_*}{\pi^4}\left[\cos\lambda_1 L_* - C_{**}\frac{\sin\lambda_1 L_*}{\sin\lambda_1} + L_*\left[C_*\cos\lambda_1 L_* + \frac{\lambda_1}{2}\sin\lambda_1 L_*\right] + (2L_* - 1)\right]$$

(for the detailed solution go through with Appendix). Consequently the transverse velocity component being calculated as:

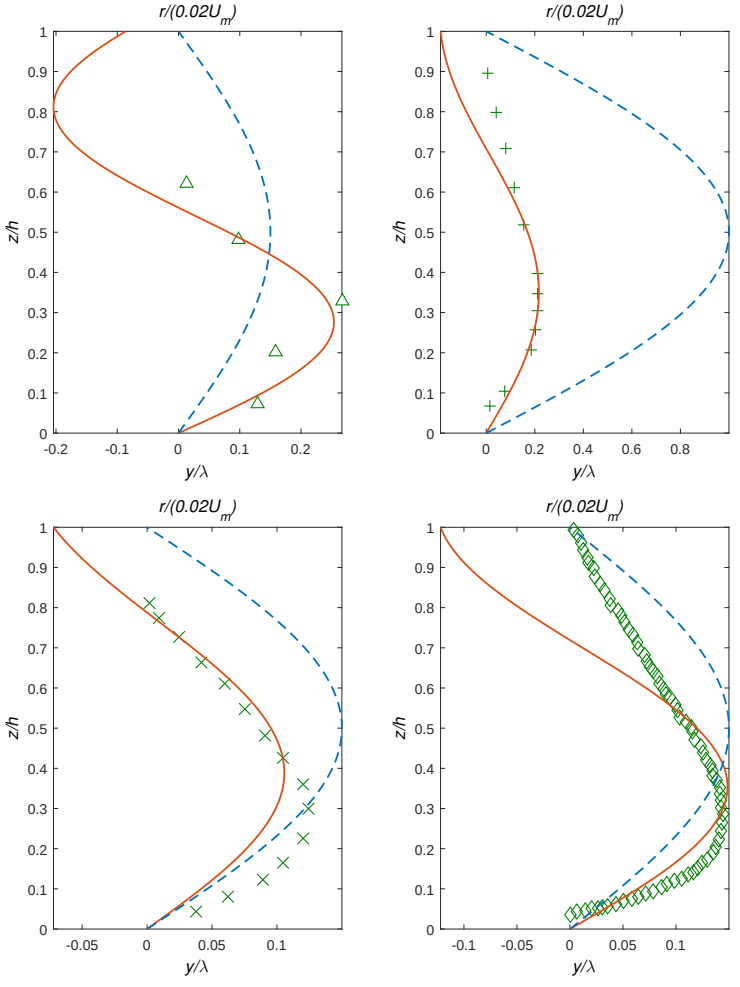

FIG. 12. Validation of the model Eq. 6.2 with experimental data of [24] and comparison with the model of [5]. Here continuous lines ('–') denote the present study, dashed lines ('– –') denote the model of [5] and symbols (◇, ×, +, △) denote data points.

$$\tilde{q} = -\frac{C_1\pi}{2L_*}\cos\left(\frac{\pi\tilde{z}}{2L_*}\right)\frac{\sin(1/2-\tilde{y}+\pi/2)\chi_1}{\chi_1\sin\frac{\chi_1}{2}} - \frac{\lambda_* L\sin(\pi\tilde{y})}{\pi^5}\left[-\lambda_1\sin(\lambda_1\tilde{z}) - \frac{\lambda_1\cos(\lambda_1\tilde{z})}{\sin\lambda_1}C_{**} + \tilde{z}\left[-\lambda_1\sin(\lambda_1\tilde{z})C_* + \frac{\lambda_1^2}{2}\cos(\lambda_1\tilde{z})\right] + \left[C_*\cos(\lambda_1\tilde{z}) + \frac{\lambda_1}{2}\sin(\lambda_1\tilde{z})\right] + 2\right]. \tag{6.3}$$

We have also validated these results with the experimental data of the [23–25].

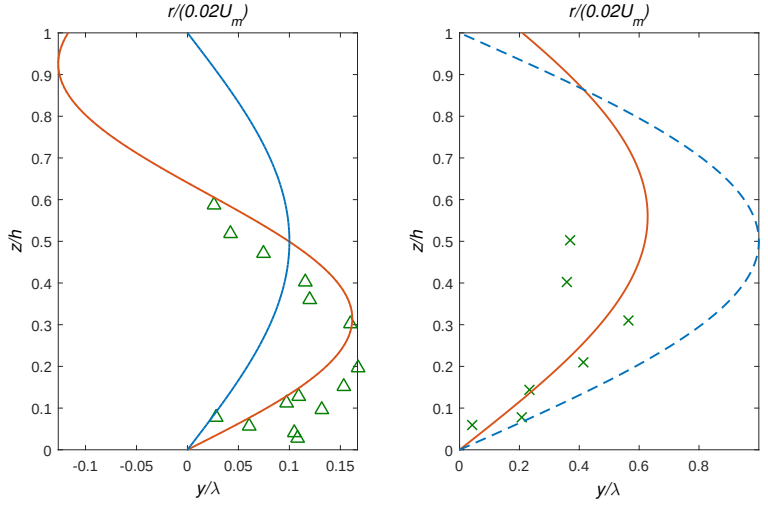

FIG. 13. Validation of the model Eq. 6.2 with experimental data of [25] and comparison with the model of [5]. Here continuous lines ('–') denote the present study, dashed lines ('– –') denote the model of [5] and symbols (△ and ×) denote data points.

TABLE 3. Details of the parameters α and L_* of proposed model in Eq. (6.2).

y/λ	L_*	α
Data of [23]		
0	0.6846	0.006
0.2	0.5664	0.006
0.8	0.5555	0.006
1.0	0.4345	0.006
Data of [25]		
0	0.3	0.0148
0	0.5650	0.0177
Data of [24]		
0	0.2666	0.013
0	0.34	0.0143
0	0.37	0.0124
0	0.34	0.0135

The results are presented in Figs. 11–13 along with the comparison with the model of [5]. In the above study α is generated from the Reynolds shear stress distribution for that case throughout the study the value of $\alpha = 0.2$. Due to the unavailability of the data of α in this case, we have considered it as a free parameter. The values of α and L_* are shown in Table 3. From the figures, it can easily be observed that the present study gives improved results. Similarly, for further study, the other cases of bed configurations can be calculated. Interested readers can further develop models corresponding to the other cases.

7. Conclusions and future scopes

The mathematical models of vertical and transverse secondary flow velocities in the steady and uniform flow through wide rectangular open channels with elevated periodic bed-forms have been proposed in this study. An absolute analytical solution of secondary flow velocities and associated stream functions observed through solving generalized governing equation (RANS equation and continuity equation) unlike the previously proposed empirical and semi-empirical models. The findings of this study are more general concerning all previously proposed models. The following conclusions are drawn from this study:

1. The governing equations are solved by using a mathematical approach and analytical solutions are obtained for different bedforms. At the very beginning, the problem is cleaved into two separate sub-problems by using the concept of linear estimation and highlighting the bed perturbation effect. The models contain the effect of fluid viscosity and eddy viscosity of turbulence. This suggests that these models can be applied for flows other than the water and can also be modified for sediment mixed flows where the spatial variation of density exists.
2. All models are validated with existing experimental data and compared to the previously proposed empirical models. The validation of the results shows that the proposed models are comparable with subsisting models and in some cases (can be observed from the error table) provide more accurate results in forecasting the perpendicular and transverse direction secondary velocity components.
3. From the analysis of the results of case S50, it is found that the circulation center changes significantly with the ratio of the length of the rough bed to the smooth bed. A least square model is proposed to calculate the location of its center of it.
4. Like previous findings, in this study it is also found that for unequal bed forms, secondary cells are being distorted laterally and for a WR-type bed structure (as given in [5]), these circular cells are distorted vertically.

5. Also from three bed configurations (S75, S50 and WR) other types of beds are considered here with elevated bedforms. It has been found that no significant vertical distortion is observed for the parabolic-type bedforms for the chosen specific bed height; whereas secondary cells are vertically distorted for triangular-type bedforms.

Till now the structure of secondary cells in the elevated wavy bed conditions are available in the literature. This study gives an idea of the structure of secondary flow cells in the other kind of elevated bed forms that can be seen in nature. The present study gives a least square model which shows how the circulation center shifts. This result can be used when some experiment regarding secondary current is performed. Furthermore, the models of secondary current can be used to study the lateral distribution of shear stress. Since the study of [34] shows that the lateral shear stress distribution depends on the secondary flows.

8. Appendix

8.1. Detailed solutions

8.1.1. Circumstantial solution of sub-problem (I). In this section the circumstantial solution of sub-problem (I) is explained. Considering the equation along with the boundary conditions such as:

$$\Sigma\frac{\partial^4\tilde{R}_1}{\partial\tilde{z}^4}+\Xi\frac{\partial^4\tilde{R}_1}{\partial\tilde{y}^2\partial\tilde{z}^2}+\Sigma\frac{\partial^4\tilde{R}_1}{\partial\tilde{y}^4}=-\tilde{\Phi}(\tilde{y},\tilde{z}). \tag{8.1}$$

The suitable boundary conditions for the sub-problem (I) are

$$\tilde{R}_1(\tilde{z}=0)=0,\quad \tilde{R}_1(\tilde{z}=1)=0,\quad \frac{\partial^2\tilde{R}_1}{\partial\tilde{z}^2}(\tilde{z}=0)=0,$$
$$\frac{\partial^2\tilde{R}_1}{\partial\tilde{z}^2}(\tilde{z}=1)=0,\quad \frac{\partial\tilde{R}_1}{\partial\tilde{z}}(\tilde{z}=1/2)=0.$$

From Eq. (3.2) $\tilde{R}_1$ can be written in the form of

$$\tilde{R}_1=F(\tilde{z})G(\tilde{y}). \tag{8.2}$$

Since the $F(\tilde{z})G(\tilde{y})$ are related to the period of perturbation where $F(\tilde{z})$ represented the amplitude of perturbation and $G(\tilde{y})$ be some periodic function represented as $G(\tilde{y})=\cos(\pi\tilde{y})$. Substituting it in Eq. (8.1) we get the fourth order non-homogeneous ordinary differential equation in the form of:

$$F''''(\tilde{z})-\frac{\Xi\pi^2}{\Sigma}F''(\tilde{z})+\pi^4F(\tilde{z})=-L(1-2\tilde{z}). \tag{8.3}$$

With the existing boundary conditions $F(0) = 0$, $F(1) = 0$, $F''(0) = 0$ and $F''(1) = 0$.

Now we define the associated homogeneous differential equation of the form:

$$F''''(\tilde{z}) - \frac{\Xi\pi^2}{\Sigma}F''(\tilde{z}) + \pi^4 F(\tilde{z}) = 0, \tag{8.4}$$

where $L = \frac{\alpha_0 \alpha \pi^3}{\Sigma}$. We know the general solution of Eq. (8.3) is of the form $F = F_c + F_p$, where F_c is the complementary solution and F_p is the particular solution. We assume that the auxiliary equation is of the form by substituting the exact solution of the form $F_c(\tilde{z}) = e^{(m\tilde{z})}$ in Eq. (8.4) we get the auxiliary equation of the form:

$$m^4 - \frac{\Xi\pi^2}{\Sigma}m^2 + \pi^4 = 0. \tag{8.5}$$

Roots of $m \simeq \pm\lambda_1 i$ where $\lambda_1 = \pi\sqrt{\frac{|\Xi|}{2\Sigma}}$. Hence the complementary solution is written in the form of:

$$F_c(\tilde{z}) = C_1\cos(\tilde{z}) + C_3\sin(\tilde{z}) + \tilde{z}[C_2\cos(\tilde{z}) + C_4\sin(\tilde{z})]. \tag{8.6}$$

To find the particular solution we apply the undetermined coefficient method which leads the form of the undetermined coefficient set $\{\tilde{z}, 1\}$, hence

$$F_p(\tilde{z}) = A_1\tilde{z} + B_1. \tag{8.7}$$

Substituting Eq. (8.7) in Eq. (8.3) we get the constants A_1 and B_1 in the form

$$A_1 = \frac{2L}{\pi^4}, \qquad B_1 = -\frac{L}{\pi^4}.$$

Hence, the final solution of Eq. (8.3) is expressed as:

$$F = C_1\cos(\tilde{z}) + C_3\sin(\tilde{z}) + \tilde{z}[C_2\cos(\tilde{z}) + C_4\sin(\tilde{z})] + \frac{L}{\pi^4}(2\tilde{z} - 1). \tag{8.8}$$

Applying the suitable boundary conditions and determining all the constant values finally we get the solution in the form of:

$$F = \frac{L}{\pi^4}\left[\cos(\lambda_1\tilde{z}) - C_{**}\frac{\sin(\lambda_1\tilde{z})}{\sin\lambda_1} + \tilde{z}\left[C_*\cos(\lambda_1\tilde{z}) + \frac{\lambda_1}{2}\sin(\lambda_1\tilde{z})\right]\right], \tag{8.9}$$

where

$$C_* = \left(\frac{2\lambda_1 - \lambda_1\sin^2(\lambda_1/2) + \frac{\lambda_1^2}{4}\sin\lambda_1 - 4\sin(\lambda_1/2)}{\lambda_1\cos\lambda_1 - \sin\lambda_1 - \lambda_1\sin^2(\lambda_1/2)}\right)$$

and

$$C_{**} = 2\cos^2(\lambda_1/2) + \lambda_1/2\sin(\lambda_1/2) - C_*\cos(\lambda_1).$$

Again final solution of $\tilde{r}_1$ can be obtained as

$$\tilde{R}_1 = \lambda_* \frac{L}{\pi^4}\cos(\pi\tilde{y}) \times \left[\cos(\lambda_1\tilde{z}) - C_{**}\frac{\sin(\lambda_1\tilde{z})}{\sin\lambda_1} + \tilde{z}\left[C_*\cos(\lambda_1\tilde{z}) + \frac{\lambda_1}{2}\sin(\lambda_1\tilde{z})\right]\right]. \tag{8.10}$$

8.1.2. Circumstantial solution of sub-problem (II). In [26] the detailed solution of the sub-problem (II) has already been shown. Therefore, the final solution of the above problem (II) for $\tilde{R}_0(\tilde{y},\tilde{z})$ is expressed considering the real part as

$$\tilde{R}_0 = \sum_{n=1}^{\infty} C_n \sin(n\pi\tilde{z})\cos(n\pi\tilde{y}). \tag{8.11}$$

Hence, the vertical velocity component of the secondary flow can be written as

$$\begin{aligned}\tilde{r} = {} & C_1\sin(\pi\tilde{z})\cos(\pi\tilde{y}) \\ & + \frac{L\lambda_*}{\pi^4}\cos(\pi\tilde{y})\left[\cos(\lambda_1\tilde{z}) - \frac{\sin(\lambda_1\tilde{z})}{\sin\lambda_1}\left[2\cos^2\left(\frac{\lambda_1}{2}\right) + \frac{\lambda_1}{2}\sin\lambda_1\right.\right. \\ & \left.\left. - \cos\lambda_1\left(\frac{2\lambda_1 - \lambda_1\sin^2(\lambda_1/2) + \frac{\lambda_1^2}{4}\sin\lambda_1 - 4\sin(\lambda_1/2)}{\lambda_1\cos\lambda_1 - \sin\lambda_1 - \lambda_1\sin^2(\lambda_1/2)}\right)\right] \right. \\ & + \tilde{z}\left[\cos(\lambda_1\tilde{z})\left(\frac{2\lambda_1 - \lambda_1\sin^2(\lambda_1/2) + \frac{\lambda_1^2}{4}\sin\lambda_1 - 4\sin(\lambda_1/2)}{\lambda_1\cos\lambda_1 - \sin\lambda_1 - \lambda_1\sin^2(\lambda_1/2)}\right)\right. \\ & \left.\left. + \frac{\lambda_1}{2}\sin(\lambda_1\tilde{z})\right] + (2\tilde{z}-1)\right].\end{aligned} \tag{8.12}$$

On the onset of instability [26, 35] the value of $n = 1$ is taken. To find the constant C_1, the boundary condition $\tilde{r}|_{|\tilde{y}|=1,\,\tilde{z}=1/2} = \widetilde{R}_{\max}$ is substituted into Eq. (8.12) which gives

$$\begin{aligned}C_1 = {} & -\widetilde{R}_{\max} \\ & - \frac{\lambda_* L}{\pi^4}\left[\frac{1}{2}\left(\frac{1+3\cos^2(\lambda_1/2)}{\cos\lambda_1/2}\right)\left(\frac{2\lambda_1 - \lambda_1\sin^2(\lambda_1/2) + \frac{\lambda_1^2}{4}\sin\lambda_1 - 4\sin(\lambda_1/2)}{\lambda_1\cos\lambda_1 - \sin\lambda_1 - \lambda_1\sin^2(\lambda_1/2)}\right)\right. \\ & \left. - \frac{\lambda_1}{4}\sin\lambda_1/2\right].\end{aligned} \tag{8.13}$$

Hence, the final solution for the vertical velocity component can be expressed as:

$$
\begin{aligned}
(8.14)\qquad \tilde{r} = \Bigg[& -\widetilde{R}_{\max} - \frac{\lambda_* L}{\pi^4}\Bigg[\frac{1}{2}\Bigg(\frac{1+3\cos^2(\lambda_1/2)}{\cos\lambda_1/2}\Bigg) \\
& \times \Bigg(\frac{2\lambda_1 - \lambda_1\sin^2(\lambda_1/2) + \frac{\lambda_1^2}{4}\sin\lambda_1 - 4\sin(\lambda_1/2)}{\lambda_1\cos\lambda_1 - \sin\lambda_1 - \lambda_1\sin^2(\lambda_1/2)}\Bigg) \\
& - \frac{\lambda_1}{4}\sin\lambda_1/2\Bigg]\Bigg]\sin(\pi\tilde{z})\cos(\pi\tilde{y}) \\
& + \frac{L\lambda_*}{\pi^4}\cos(\pi\tilde{y})\Bigg[\cos(\lambda_1\tilde{z}) - \frac{\sin(\lambda_1\tilde{z})}{\sin\lambda_1}\Bigg[2\cos^2\Bigg(\frac{\lambda_1}{2}\Bigg) + \frac{\lambda_1}{2}\sin\lambda_1 \\
& - \cos\lambda_1\Bigg(\frac{2\lambda_1 - \lambda_1\sin^2(\lambda_1/2) + \frac{\lambda_1^2}{4}\sin\lambda_1 - 4\sin(\lambda_1/2)}{\lambda_1\cos\lambda_1 - \sin\lambda_1 - \lambda_1\sin^2(\lambda_1/2)}\Bigg)\Bigg] \\
& + \tilde{z}\Bigg[\cos(\lambda_1\tilde{z})\Bigg(\frac{2\lambda_1 - \lambda_1\sin^2(\lambda_1/2) + \frac{\lambda_1^2}{4}\sin\lambda_1 - 4\sin(\lambda_1/2)}{\lambda_1\cos\lambda_1 - \sin\lambda_1 - \lambda_1\sin^2(\lambda_1/2)}\Bigg) \\
& + \frac{\lambda_1}{2}\sin(\lambda_1\tilde{z})\Bigg] + (2\tilde{z}-1)\Bigg].
\end{aligned}
$$

Similarly the transverse velocity component can be expressed as:

$$
\begin{aligned}
(8.15)\qquad \tilde{q} = & -\Bigg[-\widetilde{R}_{\max} - \frac{\lambda_* L}{\pi^4}\Bigg[\frac{1}{2}\Bigg(\frac{1+3\cos^2(\lambda_1/2)}{\cos\lambda_1/2}\Bigg) \\
& \times\Bigg(\frac{2\lambda_1 - \lambda_1\sin^2(\lambda_1/2) + \frac{\lambda_1^2}{4}\sin\lambda_1 - 4\sin(\lambda_1/2)}{\lambda_1\cos\lambda_1 - \sin\lambda_1 - \lambda_1\sin^2(\lambda_1/2)}\Bigg) \\
& - \frac{\lambda_1}{4}\sin\lambda_1/2\Bigg]\Bigg]\cos(\pi\tilde{z})\sin(\pi\tilde{y}) \\
& - \frac{\lambda_* L\sin(\pi\tilde{y})}{\pi^5}\Bigg[-\lambda_1\sin(\lambda_1\tilde{z}) - \frac{\lambda_1\cos(\lambda_1\tilde{z})}{\sin\lambda_1}\Bigg[2\cos^2\Bigg(\frac{\lambda_1}{2}\Bigg) + \frac{\lambda_1}{2}\sin\lambda_1 \\
& - \cos\lambda_1\Bigg(\frac{2\lambda_1 - \lambda_1\sin^2(\lambda_1/2) + \frac{\lambda_1^2}{4}\sin\lambda_1 - 4\sin(\lambda_1/2)}{\lambda_1\cos\lambda_1 - \sin\lambda_1 - \lambda_1\sin^2(\lambda_1/2)}\Bigg)\Bigg] \\
& + \tilde{z}\Bigg[-\lambda_1\sin(\lambda_1\tilde{z})\Bigg(\frac{2\lambda_1 - \lambda_1\sin^2(\lambda_1/2) + \frac{\lambda_1^2}{4}\sin\lambda_1 - 4\sin(\lambda_1/2)}{\lambda_1\cos\lambda_1 - \sin\lambda_1 - \lambda_1\sin^2(\lambda_1/2)}\Bigg) + \frac{\lambda_1^2}{2}\cos(\lambda_1\tilde{z})\Bigg] \\
& + \Bigg[\cos(\lambda_1\tilde{z})\Bigg(\frac{2\lambda_1 - \lambda_1\sin^2(\lambda_1/2) + \frac{\lambda_1^2}{4}\sin\lambda_1 - 4\sin(\lambda_1/2)}{\lambda_1\cos\lambda_1 - \sin\lambda_1 - \lambda_1\sin^2(\lambda_1/2)}\Bigg) + \frac{\lambda_1}{2}\sin(\lambda_1\tilde{z})\Bigg] + 2\Bigg].
\end{aligned}
$$

8.1.3. Calculation of sub-problem (II) following discussion. In [27] already shown the method of finding the solution for the detailed solution of this type of a problem. Apart from this by using the new boundary conditions of Eq. (6.1) we get $\tilde{R}_0$ as:

$$\tilde{R}_0 = C_1 \frac{\sin(0.5-\tilde{y})\chi_1}{\sin(0.5\chi_1)} \sin\left(\frac{\pi\tilde{z}}{2L_*}\right). \tag{8.16}$$

Hence the final solution of vertical velocity component is going to be in the form of:

$$\begin{aligned}\tilde{r} = {} & C_1 \sin\left(\frac{\pi\tilde{z}}{2L_*}\right) \frac{\cos(1/2-\tilde{y}+\pi/2)\chi_1}{\sin\frac{\chi_1}{2}} \\ & + \lambda_* \frac{L}{\pi^4} \cos(\pi\tilde{y}) \left[\cos(\lambda_1\tilde{z}) - C_{**} \frac{\sin(\lambda_1\tilde{z})}{\sin\lambda_1}\right. \\ & \left. + \tilde{z}\left[C_* \cos(\lambda_1\tilde{z}) + \frac{\lambda_1}{2}\sin(\lambda_1\tilde{z})\right] + (2\tilde{z}-1)\right].\end{aligned} \tag{8.17}$$

Now applying the boundary conditions $\tilde{r}|_{|\tilde{y}|=1,\,\tilde{z}=L_*} = \widetilde{R}_{\max}$. The constant term C_1 is in the form of:

$$\begin{aligned}C_1 = {} & -\widetilde{R}_{\max} - \frac{L\lambda_*}{\pi^4}\left[\cos\lambda_1 L_* - C_{**}\frac{\sin\lambda_1 L_*}{\sin\lambda_1}\right. \\ & \left. + L_*\left[C_*\cos\lambda_1 L_* + \frac{\lambda_1}{2}\sin\lambda_1 L_*\right] + (2L_*-1)\right].\end{aligned} \tag{8.18}$$

Finally, from the continuity equation the transverse velocity component has been calculated as following:

$$\tilde{q} = -\int \frac{\partial\tilde{r}}{\partial\tilde{z}}\, d\tilde{y} \tag{8.19}$$

and we get

$$\begin{aligned}\tilde{q} = {} & -\frac{C_1\pi}{2L_*}\cos\left(\frac{\pi\tilde{z}}{2L_*}\right)\frac{\sin(1/2-\tilde{y}+\pi/2)\chi_1}{\chi_1\sin\frac{\chi_1}{2}} \\ & - \frac{\lambda_* L\sin(\pi\tilde{y})}{\pi^5}\left[-\lambda_1\sin(\lambda_1\tilde{z}) - \frac{\lambda_1\cos(\lambda_1\tilde{z})}{\sin\lambda_1}C_{**}\right. \\ & + \tilde{z}\left[-\lambda_1\sin(\lambda_1\tilde{z})C_* + \frac{\lambda_1^2}{2}\cos(\lambda_1\tilde{z})\right] \\ & \left. + \left[C_*\cos(\lambda_1\tilde{z}) + \frac{\lambda_1}{2}\sin(\lambda_1\tilde{z})\right] + 2\right].\end{aligned} \tag{8.20}$$

For further study the interested person can go through with the above calculations which shows other elevated and non-elevated channel cases.

Conflict-of-Interest

Authors declare no conflict of interest.

Author Contributions

S.K. initiated the idea of the work and edited the paper. T.C. (Ph.D. student) has performed the calculation, simulation, plotting, and prepared the draft. Both of the authors revised the paper and prepared the final version.

Acknowledgements

We express our sincere thanks to Prof. Jacek Pozorski, Section Editor, and the anonymous reviewers for their constructive and useful comments which have improved the revised version of the paper.

References

1. L. Prandtl, *Essentials of Fluid Mechanics*, Blackie & Son Ltd, London and Glasgow, 1952.
2. I. Nezu, W. Rodi, *Experimental study on secondary currents in open channel flow*, [in:] 21th IAHR Congress, IAHR, Melbourne, pp. 115–119, 1985.
3. S. Ikeda, *Self forced straight channels in sandy beds*, Journal of Hydraulic Division, **107**, 389–406, 1981.
4. I. Nezu, H. Nakagawa, *Turbulence in Open-Channel Flows*, IAHR Monograph, Balkema, Rotterdam, The Netherlands, 1993.
5. Z. Wang, N. Cheng, *Time-mean structure of secondary flows in open channel with longitudinal bedforms*, Advances in Water Resources, **29**, 1634–1649, 2006.
6. V.T. Chow, *Open-Channel Hydraulics*, Civil Engineering Series, McGraw-Hill, 1959.
7. F. Stearns, *On the current meter, together with a reason why the maximum velocity of water flowing in open channel is below the surface*, Transactions of ASCE, **12**, 331–338, 1983.
8. J. Francis, *On the cause of the maximum velocity of water flowing in open channels being below the surface*, Transactions of ASCE, **7**, 109–113, 1878.
9. A. Gibson, *On the depression of the filament of maximum velocity in a stream flowing through an open channel*, Proceedings of the Royal Society A, Mathematical and Physical Sciences, **82**, 149–159, 1909.
10. J. Thomson, *On the origin of windings of rivers in alluvial plains, with remarks on the flow of water round bends in pipes*, Proceedings of the Royal Society of London, **25**, 5–8, 1876.
11. D. Naot, W. Rodi, *Calculation of secondary currents in channel flow*, Journal of Hydraulic Division, **108**, 948–968, 1982.

12. F. GESSNER, *The origin of secondary flow in turbulent flow along a corner*, Journal of Fluid Mechanics, **58**, 1–25, 1973.

13. Z. WANG, N. CHENG, *Time-mean structure of secondary flows in open channel with longitudinal bedforms*, Advances in Water Resources, **29**, 1634–1649, 2006.

14. Z. WANG, N. CHENG, *Secondary flows over artificial bed strips*, Advances in Water Resources, **28**, 441–450, 2005.

15. I. NEZU, H. NAKAGAWA, *Cellular secondary currents in straight conduit*, Journal of Hydraulic Engineering, **110**, 173–193, 1984.

16. V. VANONI, *Transportation of suspended sediment by running water*, Transactions of ASCE, **111**, 67–133, 1946.

17. J. COLEMAN, *Brahmaputra river; channel process and sedimentation*, Sedimentary Geology, **3**, 129–239, 1969.

18. R. KINOSHITA, *An analysis of the movement of flood waters by aerial photography; concerning characteristics of turbulence and surface*, Photographic Surveying, **6**, 1–17, 1967 [in Japanese].

19. S. YANG, S. TAN, S. LIM, *Velocity distribution and dip-phenomenon in smooth uniform open channel flows*, Journal of Hydraulic Engineering, **130**, 1179–1186, 2004.

20. S.Q. YANG, *Interactions of boundary shear stress, secondary currents and velocity*, Fluid Dynamics Research, **36**, 121–136, 2005.

21. S. KUNDU, K. GHOSHAL, *An analytical model for velocity distribution and dip-phenomenon in uniform open channel flows*, International Journal of Fluid Mechanics Research, **39**, 381–395, 2012.

22. S. MOHAN, S. KUNDU, K. GHOSHAL, J. KUMAR, *Numerical study on two dimensional distribution of streamwise velocity in open channel turbulent flows with secondary current effect*, Archieves of Mechanics, **73**, 175–200, 2021.

23. T. OHMOTO, Z. CUI, R. HIRAKAWA, *Effects of secondary currents on suspended sediment transport in an open channel flow*, [in:] G. Jirka, W. Uijttewaal [eds.], International Symposium on Shallow Flows, Delft, Netherlands, pp. 511–516, 2004.

24. A. SOUALMIA, S. ZAOUALI, C. LABIOD, *Modeling of secondary motions driven by the turbulence anisotropy in closed and open channels*, Lebanese Science Journal, **9**, 75–89, 2008.

25. K. GHOSHAL, R. MAZUMDER, C. CHAKRABORTY, B. MAZUMDER, *Turbulence, suspension and downstream fining over a sand-gravel mixture bed*, International Journal of Sediment Research, **28**, 194–209, 2013.

26. S. KUNDU, T. CHATTOPADHYAY, J.H. PU, *Analytical models of mean secondary velocities and stream functions under different bed-roughness configurations in wide open-channel turbulent flows*, Environmental Fluid Mechanics, **22**, 169–188, 2022.

27. S. KUNDU, T. CHATTOPADHYAY, *Analysis and validation of mathematical models of secondary velocities along vertical and transverse directions in wide open-channel turbulent flows*, Fluid Dynamics Research, **54**, 1–31, 2022.

28. J. HINZE, *Turbulence*, McGraw-Hill, New York, 1975.

29. J. Guo, *Self-similarity of mean flow in pipe turbulence*, in: 36th AIAA Fluid Dynamics Conferences and Exhibit, AIAA paper 2885, San Francisco, CA, 2006.

30. S. Kundu, *Theoretical study on velocity and suspension concentration in turbulent flow*, Ph.D. Thesis, Indian Institute of Technology Kharagpur, West Bengal, India, 2015.

31. N. Patel, J. Shahi, J. Guo, *Applications of second log-wake law for turbulent velocity distributions in laboratory flumes and natural rivers*, Journal of Hydraulic Engineering, **147**, 1–8, 2021.

32. S.Q. Yang, S.K. Tan, X.K. Wang, *Mechanism of secondary currents in open channel flows*, Journal Of Geophysical Research, **117**, 1–13, 2012.

33. X. Studerus, *Sekundärströmungen im offenen gerrinne über rauhen längsstreifen*, Ph.D. Thesis, Institut für Hydromechanik und Wasserwirtschaft, ETH, Zürich, Switzerland, 1982.

34. J. Guo, P.Y. Julien, *Shear stress in smooth rectangular open-channel flows*, Journal of Hydraulic Engineering, **131**, 30–37, 2005.

35. N.E. Kotsovinos, *Secondary currents in straight wide channels*, Applied Mathematics Modelling, **12**, 22–24, 1988.

Received September 3, 2022; revised version March 23, 2023.
Published online May 5, 2023.